



Long-term analysis of atmospheric propane over Southern Europe based on observations conducted at the WMO-GAW station of Monte Cimone

Enrico Mancinelli¹, Saurabh Annadate^{1,2}, Paolo Cristofanelli², Umberto Giostra¹, Michela Maione^{1,2}, Stefan Reimann³, and Jgor Arduini^{1,2}

Correspondence: Jgor Arduini (jgor.arduini@uniurb.it)

Abstract. This study presents the analysis of a 13-year time series of continuous measurements of propane (C₃H₈) from the WMO-GAW station of Monte Cimone (CMN, Italy) between 2011 and 2023. Background trend and pollution events are evaluated to establish how this remote site is influenced by regional and/or global emissions. C₃H₈ background mixing ratios did not substantially vary over the study period with a slight decrease of -0.003 [-0.004; -0.002; 95% confidence interval] ppb per year. However, C₃H₈ seasonal amplitude showed an increase of about 0.16% per year from 77.5 to 79.5% in the study period, with most of the increase between 2016 and 2023. Based on back-trajectory sensitivity analysis, CMN and JFJ were found to be predominantly influenced by air masses originating from the central European continent and the western Mediterranean basin. Using the 2022 observations of CMN and Jungfraujoch (Switzerland) stations, and the Flexpart-Flexinvert inverse modeling framework, we estimated the distribution of regional emissions and compared it with the EDGAR bottom-up emission inventory. In particular, for Italy and France, prior emissions of C₃H₈ were underestimated by a factor of 3 and 2, respectively, likely due to overlooked C₃H₈ emissions sources and/or inaccurate activity data used to compile the bottom-up inventory.

1 Introduction

Atmospheric propane (C_3H_8) can affect both climate and air quality through the formation of tropospheric ozone and carbonyl compounds, eventually leading to secondary organic aerosols (Rosado-Reyes and Francisco, 2007). According to Hodnebrog et al. (2018), the indirect radiative forcing of C_3H_8 is about 99.3% of its total positive radiative forcing through the interactions with O_3 formation and CH_4 removal. Previous studies (Helmig et al., 2016; Angot et al., 2021; Li et al., 2022; Toon et al., 2021) informed about variations in the trends of the C_3H_8 mixing ratio in the northern hemisphere in the second decade of this century, with changes in the mixing ratio depending on the location with respect to the main sources of anthropogenic emissions, the time range considered and the sampling region (upper troposphere vs. lower stratosphere). Variations in C_3H_8 mixing ratios were reported with seasons (Helmig et al., 2015) and latitude (Helmig et al., 2014, 2016) at remote measurement stations.

¹Department of Pure and Applied Sciences, University of Urbino "Carlo Bo", Urbino, Italy

²Institute of Atmospheric Sciences and Climate, National Research Council, Bologna, Italy

³Laboratory for Air Pollution / Environmental Technology, Empa, Swiss Federal Laboratories for Materials Science and Technology, Überlandstrasse 129, 8600 Dübendorf, Switzerland





Propane emissions result from natural gas and oil activities (Lan et al., 2019) due to fugitive emissions, the practices of gas venting and flaring (https://www.worldbank.org/en/programs/gasflaringreduction/methane-explained), offshore oil loading (Riddick et al., 2019), as well as burning of agricultural residue (Joshi et al., 2024). Several articles (Dalsøren et al., 2018; Bourtsoukidis et al., 2020; Rowlinson et al., 2024; Ge et al., 2024; Tzompa-Sosa et al., 2019) suggested that missing sources of anthropogenic C₃H₈ emissions (oil and gas activities) or geologic origins could explain the bias between modelled and observed mixing ratios. According to Derwent et al. (2017), the estimates of C₃H₈ emissions from natural gas leakage were biased low in the UK national emission inventory. For the Arabian Peninsula, the discrepancies between the modelled and observed non-methane hydrocarbons may be explained by the degassing of C₃H₈ from the northern Red Sea with emissions comparable to those of the Middle East countries (Bourtsoukidis et al., 2020). Several articles (Lyon et al., 2021; Thorpe et al., 2023; Serrano-Calvo et al., 2023) associated a general decrease in anthropogenic emissions from oil and gas activities in North America with the COVID-19 pandemic and the related economic crisis.

The Mediterranean basin is one of the climate change hotspots due to the consistent number of observed impacts related to climate change and the projected hazards, vulnerability, and risks associated with future scenarios of global increase in temperature (Ali et al., 2022). Therefore, it is urgent to study atmospheric composition in relation to climate-altering compounds and their precursors. This paper aims to analyse the causes that affect the background values of propane in the South European troposphere.

The analysis is based on a 13-year time series of continuous measurements of C_3H_8 , carried out at the Italian Climate Observatory 'Ottavio Vittori, a research infrastructure managed by the Institute of Atmospheric Sciences and Climate (ISAC) of the National Research Council (CNR) of Italy, within the framework of the European Research Infrastructure ACTRIS (Aerosol, Clouds, and Trace Gases), dedicated to the observation and understanding of short-lived atmospheric constituents and their interactions. Continuous measurements of CO and CH_4 at the same site are also carried out in the framework of the Integrated Carbon Observation System Research Infrastructure (ICOS-RI). The location of this observatory allows for the study of the evolution of C_3H_8 mixing ratios in the free troposphere of the Mediterranean basin and the emission sources located in the Po Valley. The diurnal and seasonal variability in the C_3H_8 mixing ratios was estimated for the study period. Variations due to the COVID pandemic and high mixing ratio events were analysed. Air mass footprints for Monte Cimone were investigated using FLEXible PARTicle (FLEXPART) (Bakels et al., 2024), a Lagrangian particle dispersion model. The seasonal sensitivity maps of air masses were compared with the sensitivity map calculated for high propane emission episodes.

2 Materials and methods

50

2.1 Propane, carbon monoxide, and methane datasets

The time frame of this study covered the period from January 2011 to December 2023. In situ online measurements were performed at the WMO/GAW global station on Monte Cimone (CMN, 44°12′ N, 10°42′ E, 2165 m above sea level). Lo Vullo et al. (2016) observed that the measurements of non-methane volatile organic compounds performed at this station are generally representative of emissions occurring in the European continent. Measurements of C₃H₈ were performed every 2 hours





with a gas chromatograph-mass spectrometer (GC–MS Agilent 6820 + Agilent 5975C) system preceded by online sample enrichment using the commercial preconcentration system Markes International Unity-2-AirServer-2, following a method described in Maione et al. (2013). Ambient air measurements are regularly calibrated against a 500 ppt "30-compounds Ozone precursor mixture" standard in nitrogen from the National Physical Laboratory (NPL-UK). Open-access C₃H₈ mole fraction data are available from the EBAS website (https://ebas.nilu.no/). Measurements of CH₄ (Cristofanelli et al., 2025a) and CO (Cristofanelli et al., 2025b) are available from the ICOS-RI "Carbon Portal" (https://data.icos-cp.eu/portal/).

2.2 Meteorological dataset

The meteorological variables (air temperature, pressure, relative humidity, and wind speed) recorded from January 2011 to December 2023 were analysed. Raw data were averaged over a 1-minute period. Between 2011 and 2014, the 1-minute data were averaged over 30-minute periods. Starting in 2015, they were averaged every hour. For the period 2011-2014, the data can be accessed through the NextData database (http://nextdata.igg.cnr.it:8080/geonetwork/srv/eng/catalog.search#/metadata/787c1a26-b92a-4d7d-9d03-8a2531980c52). For the time range 2015–2023, the hourly measurements were downloaded from the EBAS website (https://ebas.nilu.no/). Specific humidity (SH) was calculated based on air temperature, pressure, and relative humidity data. Figure A1 shows a clear diurnal trend for SH, wind speed, and temperature irrespective of the seasons. Hourly mean values of wind speed were the lowest between 11:00 and 13:00 (Fig. A1b), whereas hourly mean values of temperature and SH were the highest in the early/ mid-afternoon (between 13:00 and 16:00) (Fig. A1d, f). These figures are in line with previous work by Cristofanelli et al. (2021b) who investigated variations in wind speed, SH, and CO ambient levels as proxies of wind regime and vertical transport at Monte Cimone. The diurnal variation of SH specular to that of the wind speed may be related to the vertical transport/advection of air masses from the planetary boundary layer at Monte Cimone (Cristofanelli et al., 2016) between spring and autumn (Cristofanelli et al., 2015).

75 2.3 Statistical analysis

To evaluate seasonal cycle and trend, curve fitting of the propane dataset was performed according to the curve fitting method for CO₂ measurements (https://www.esrl.noaa.gov/gmd/ccgg/mbl/crvfit/crvfit.html accessed 14 October 2024), as done in previous studies on non-methane hydrocarbons by Angot et al. (2021) and Helmig et al. (2014). The curve fitting is based on a function fit to the data with a polynomial function for the long-term growth and harmonics for the annual oscillation. To account for interannual and short-term variations, the filtering of residuals is based on a fast Fourier transform according to Thoning et al. (1989). The trend consists of the polynomial part of the function fit together with the filtered residuals with the seasonal cycle removed, and the long-term cutoff value of 667 days. The smoothed curve is obtained by combining the results of the function fit and the results of the filter with a short-term cutoff value of 30 days.



100

105

110



2.4 Sensitivity to air masses starting at Monte Cimone

The source-receptor relationship (also referred to as sensitivity) of air masses arriving at Monte Cimone was calculated using FLEXPART v11 (Bakels et al., 2024). FLEXPART simulated the backward transport of virtual air tracer particles released from the receptor site, using wind fields from the European Centre for Medium-Range Weather Forecasts (ECMWF) ERA5 reanalysis. The sensitivity of the receptor to each grid cell is based on the average time that air parcels, traced backward from the receptor, spend in that cell. Only the sensitivity within the model height of 0-500m was included in the calculation, based on the assumption that emissions primarily occur near the ground within this layer. 10,000 particles were released every 3 hours from Monte Cimone (44.12° N, 10.42° E, 2000 m a.s.l.) and tracked backward in time for 5 days over the global domain. FLEXPART was driven by ERA5 reanalysis data with a horizontal resolution of 0.5° (Hersbach et al., 2023). Sensitivity calculations were conducted for the year 2022, during which the mean seasonal fetch regions were derived and are presented in Fig. 7. The choice of 2022 was motivated by the presence of multiple high-mixing ratio episodes that persisted for more than 2–3 days across various seasons. These prolonged episodes provided sufficient temporal coverage and variability, making 2022 a representative year for analysing the transport patterns and potential source regions influencing observations at Monte Cimone.

2.5 Emission estimation using atmospheric inversion method

The inversion of C₃H₈ emissions for 2022 was conducted using the FLEXPART-FLEXINVERT Bayesian inversion framework. In brief, FLEXINVERT (Thompson and Stohl, 2014)Bayesian inversion optimises the emission fluxes constrained by atmospheric observations, a priori inventories, and the atmospheric transport model, accounting for their respective uncertainties. To improve the sensitivity and representativeness of the inversion, propane data from Monte Cimone were complemented with measurements performed at Jungfraujoch (JFJ, Switzerland), within the framework of ACTRIS activities, and were assimilated into the inversion. The FLEXPART-FLEXINVERT inversion system has been previously implemented, validated, and extensively used for long-lived compounds such as hydrofluorocarbons using observations from CMN and JFJ (Annadate et al., 2023, 2025). Annadate et al. (2023) observed a decrease in the uncertainties of posterior emission fluxes by adding more observations from different receptors for inversions of a fluorinated trace gas over the European domain. In this study, bottom-up C₃H₈ emissions from the EDGARv8.1 inventory (https://edgar.jrc.ec.europa.eu/index.php/dataset_ap81) were used as the prior. EDGAR provides annual, sector-specific gridded fluxes for power generation, industrial combustion, buildings, transport, agriculture, fuel exploitation, industrial processes, and waste, which were aggregated to form the prior flux field for the inversion. Background mixing ratios for CMN and JFJ were estimated following Stohl's method (Stohl et al., 2009), which used FLEXPART sensitivities and prior emissions. Detailed description of Stohl's method, implementation, and comparison with other background estimation methods can be found in Stohl et al. (2009) and Vojta et al. (2022).

For the inversion, observations from CMN and JFJ were averaged to a 3-hourly temporal resolution. FLEXPART sensitivities were computed at the same 3-hourly intervals by releasing 10,000 particles and tracking them backwards in time for 10 days. Considering the short lifetime of propane, OH reactivity was included in the model. Chemical loss due to reaction with the





OH radical is represented in FLEXPART as a first-order linear process. The corresponding mass loss, m, is calculated at each timestep as

$$m(t + \Delta t) = m(t)e^{-\kappa \Delta t} \tag{1}$$

120 where the temperature-dependent reaction rate constant, $\kappa(s^{-1})$, was expressed as

$$\kappa = CT^N e^{-D/T} C_{OH} \tag{2}$$

with T being the absolute temperature and C_{OH} the hourly OH concentration. The reaction constants C, D, and N were chosen to be 7.6×10^{-12} cm³ molecule⁻¹ s⁻¹, 585K, and 0, respectively (Atkinson et al., 2006). In FLEXPART, the OH distribution is represented using monthly mean fields at a horizontal resolution of $3^{\circ} \times 5^{\circ}$ with 17 vertical levels, derived from the GEOS-Chem model. To incorporate hourly variability, these fields are scaled using the hourly ozone photolysis rate. The adjustment applies a simple parameterisation that accounts for the solar zenith angle under cloud-free conditions, thereby introducing an hourly modulation of OH concentrations (Bakels et al., 2024).

3 Results

3.1 Time series and long-term trend in C₃H₈ atmospheric mixing ratio

Figure 1 shows hourly measurements of C₃H₈ mixing ratios measured at Monte Cimone, and the estimated smooth curve and trend curve from 2011 to 2023. The time series of the C₃H₈ hourly measurements shows a clear seasonal cycle (Fig. 1). Apart from local minima and maxima of C₃H₈ mixing ratios, no clear long-term trend can be inferred with a slight decrease of -0.003 [-0.004; -0.002; 95% confidence interval] ppb per year between 2011 and 2023 (Fig. 1, green line and Fig. 2, solid black and red lines). It is worth pointing out a steep decrease in C₃H₈ long-term trend curve by -0.045 [-0.049; -0.042] ppb from May 2018 to February 2020, as well as a steep increase by 0.057 [0.053; 0.062] ppb between October 2021 and February 2023. Similar rapid changes in C₃H₈ mixing ratios are listed in the literature (Helmig et al., 2016; Angot et al., 2021). In this context, between 2011 and mid-2014 Helmig et al. (2016) documented an increase in atmospheric C₃H₈ mixing ratios in regions of the United States experiencing a rapid expansion of oil and natural gas (O&NG) extraction activities, as well as in areas in the Northern Hemisphere affected by these emission source regions. Moreover, Angot et al. (2021) observed a significant increase of C₃H₈ mixing ratio for the same period followed by a decrease from July 2014 to July 2016 and then a substantial stable concentration for the 2016-2019 period, confirmed by independent discrete sampling by NOAA/GML networks. These authors pointed at US O&NG activities as the most likely driver responsible for the change in total emissions and for baseline atmospheric levels in the northern hemisphere, rather than changes in OH sinks or BB emissions. Direct comparison with long-term trends derived from multiple background sites reported by Angot et al. (2021) clearly shows (Fig. 2) an uncorrelated variability among sites, suggesting that local perturbations on emissions are not clearly affecting trends at the global scale that are likely driven by temporal variation on emissions at the hemispheric scale.





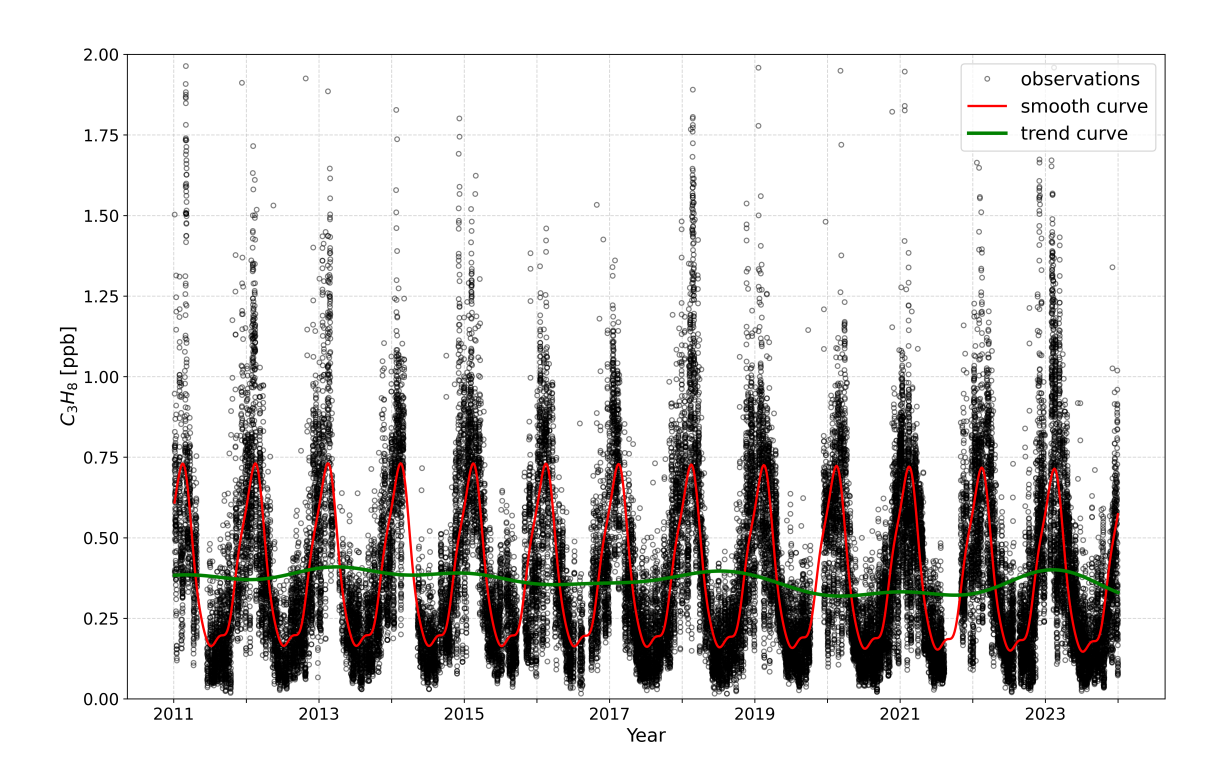


Figure 1. Smooth curve, trend curve, and timeseries of propane hourly mixing ratios measured at Monte Cimone (Italy) from 2011 to 2023.

3.2 Seasonal variations in C_3H_8 mixing ratios

150

155

Figure 3 shows monthly mean values of C_3H_8 mixing ratios measured at Monte Cimone from 2011 to 2023. The highest monthly means of C_3H_8 mixing ratios were measured between January and March, with values in the range of 0.610–0.724 ppb (Fig. 3). The lowest monthly means of C_3H_8 mixing ratios occurred between June and September, with values in the range of 0.169–0.203 ppb (Fig. 3). Variability in C_3H_8 mixing ratios was higher in cold months and lower in hot months (Fig. A2). Our results are in line with the findings by Helmig et al. (2015) and Helmig et al. (2016), who observed atmospheric nonmethane hydrocarbon mixing ratios measured at several remote global sampling sites peaking in late winter and decreasing in summer for the Northern Hemisphere over a 10-year range. In the work by Debevec et al. (2021), analysis of volatile organic compounds in a remote Mediterranean background site in Corsica (France) showed that the ambient mixing ratios of C_3H_8 were 4.3 times higher in winter than in summer. Moreover, these authors pointed out that the C_3H_8 mixing ratios had low summer values and high winter values spread over relatively narrow and wide ranges, respectively. Seasonal changes in C_3H_8 reactivity with OH (Helmig et al., 2014, 2016) and emission sources (Kim et al., 2015) play a role in the variations in atmospheric C_3H_8 mixing ratios. The main atmospheric sink of C_3H_8 is through the reaction with OH, whose tropospheric abundance is driven





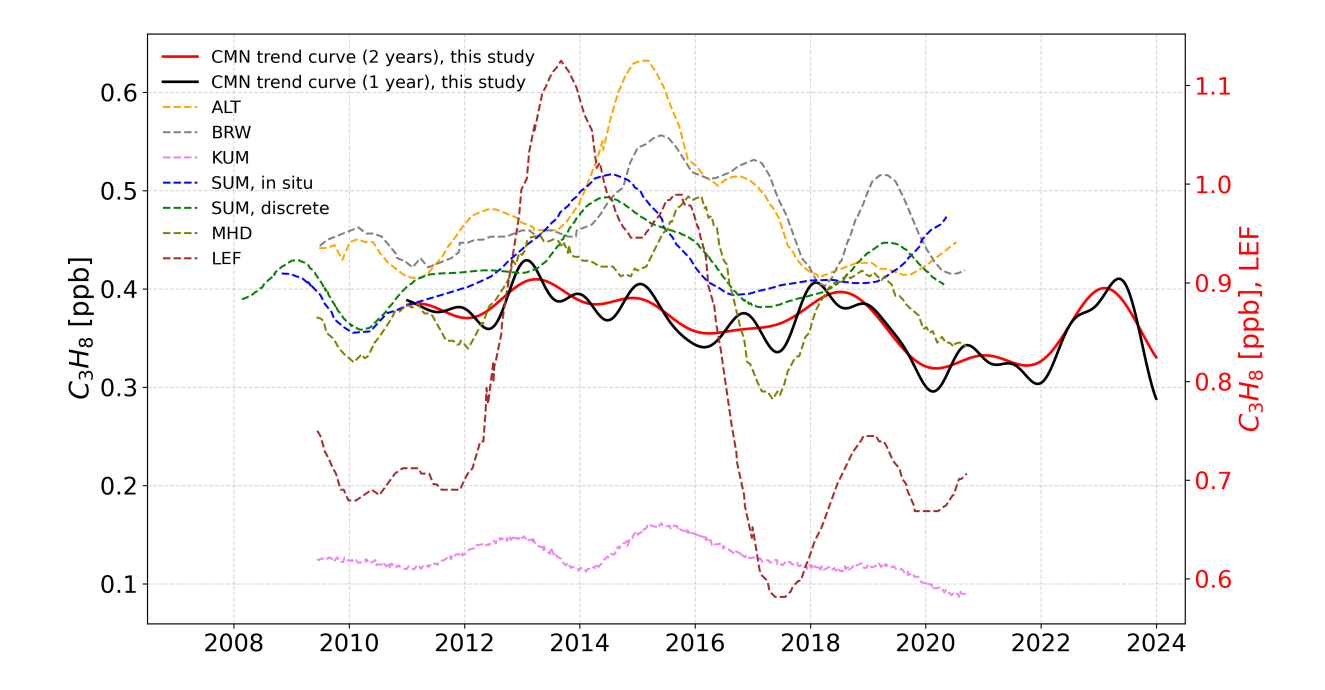


Figure 2. Comparison of the trend curve of propane mixing ratios measured at Monte Cimone (Italy) (solid lines) with those reported by Angot et al. (2021) (dashed lines).

by a complex series of chemical reactions involving tropospheric ozone, methane, carbon monoxide, NMHCs, and nitrogen oxides and by atmospheric variables varying with the seasons, namely the levels of solar radiation and humidity (Helmig et al., 2016). Moreover, gas consumption in the EU is higher in the cold months compared to the hot months (Energy, 2025). In addition, throughout the year, the propane/butane gas mixture changes in liquefied petroleum gas with generally higher ratios of propane/butane in winter compared to summer (Kim et al., 2015). This is done to improve the start ability of engines fueled with liquefied petroleum gas during the cold season (Baek et al., 2022). Hu et al. (2025) reported a seasonal pattern with higher C₃H₈ emissions in winter compared to summer for the O&NG production regions of the United States.

Changes in the seasonal cycle of C_3H_8 are affected by emissions, the atmospheric OH sink, and atmospheric transport. Following previous studies (Angot et al., 2021; Dlugokencky et al., 1997), for each year, the amplitude (peak-to-minimum) of the propane seasonal cycle was calculated as the relative difference between the maximum and minimum values of the smoothed curve (red line in Fig. 1) of the C_3H_8 measured mixing ratios. Between 2011 and 2023, the trend line shows an increase of about 0.16% per year in the relative amplitude, with values in the range of 77.5–79.5% (Fig. 4). Specifically, the increase in C_3H_8 seasonal amplitude occurred between 2016 and 2023, whereas there were no substantial variations in the relative amplitude yearly values between 2011 and 2014. The 95% confidence interval refers to 30 iterations performed



180



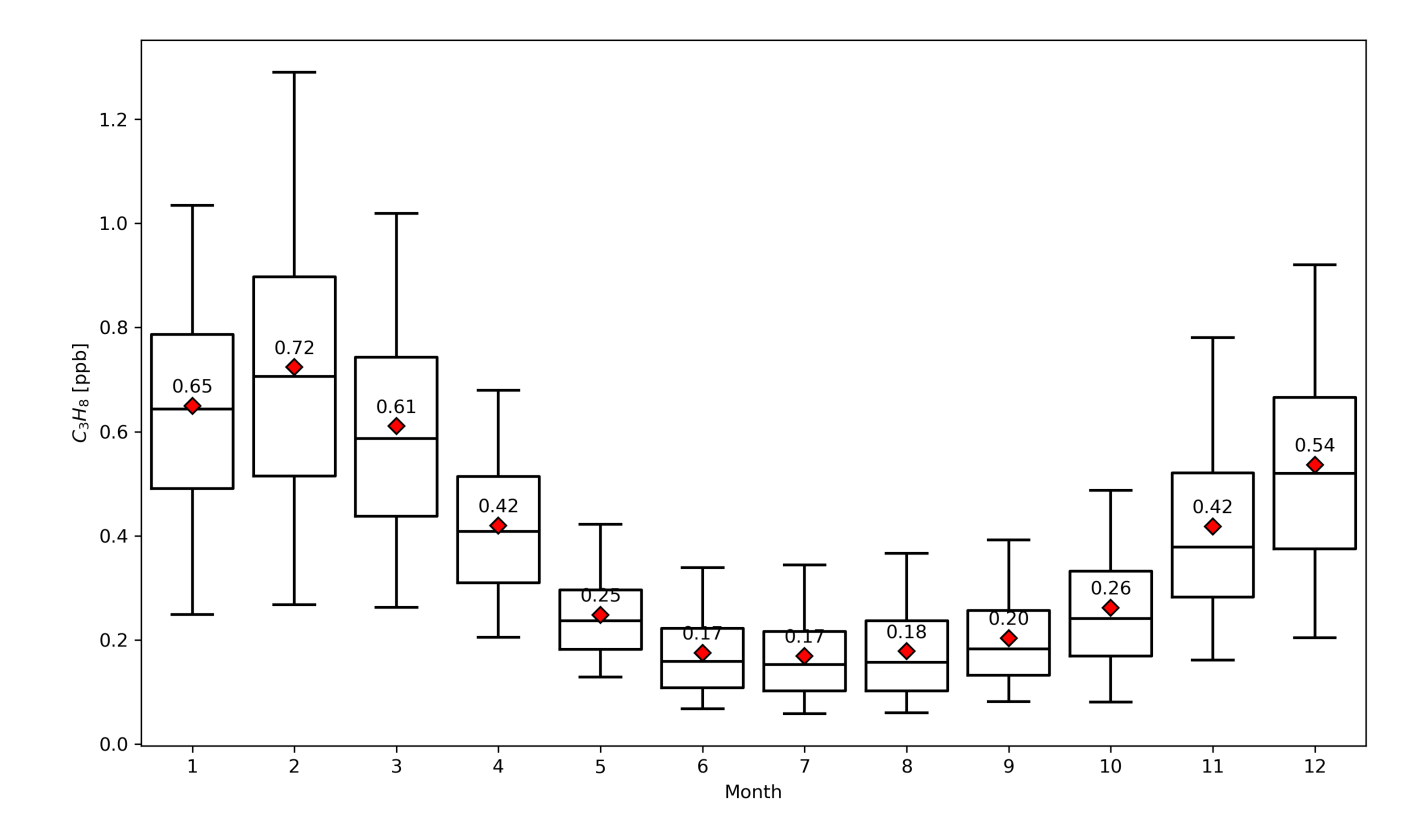


Figure 3. Boxplots of C_3H_8 mixing ratios measured at Monte Cimone (Italy) grouped by month from 2011 to 2023. From bottom to top, the horizontal lines of the boxplots show the minimum, 25%, 50%, and 75% percentiles of the data, and the maximum. Red diamonds show mean values.

on subsets consisting of 80% of the dataset. Based on C₃H₈ measurements in Greenland in the time ranges 2008–2010 and 2012–2020, Angot et al. (2021) reported relative amplitudes in the range of 92–96% and an increase in relative amplitudes of 0.17% per year, although not statistically significant. The removal of C₃H₈ from the atmosphere varies with solar irradiance and thus with the latitude of the measurement station (Helmig et al., 2014, 2016). Therefore, differences in the amplitude of the seasonal cycle of C₃H₈ can be explained by differences in latitudinal locations between this study and the study by Angot et al. (2021). A similar discussion on changes in seasonal amplitude for atmospheric methane was reported by Liu et al. (2025), for which the increasing trend in mid-low latitudes is dominated by an enhanced CH₄ sink driven by a positive trend of tropospheric OH concentration, most likely due to increases in anthropogenic NOx emissions and decreases in CO emissions. Previous studies observed negative trends in CO concentrations based on remote sensing (Elshorbany et al., 2024) and ground-based (Gialesakis et al., 2023) observations in the Mediterranean basin in the last two decades. Carbon monoxide is the main sink for OH in the troposphere (Lelieveld et al., 2016), so that long-term reductions in CO could result in higher OH abundance (Zhao et al., 2020), albeit the large uncertainties in modeling OH sinks and sources (Lelieveld et al., 2016). Therefore, the trend





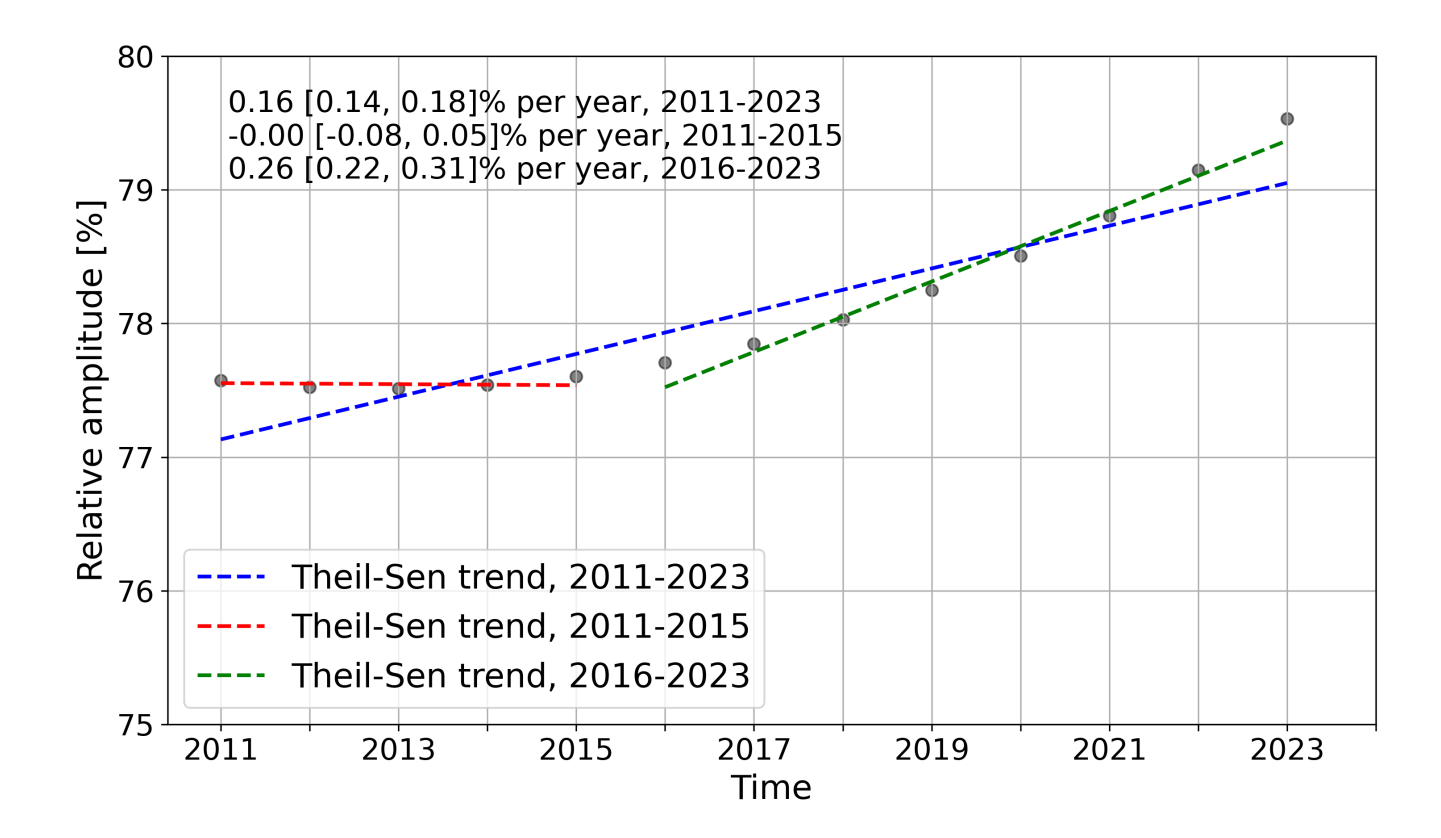


Figure 4. The trend line of propane seasonal amplitude at Monte Cimone (Italy) was calculated using minimum and maximum values of the smoothed curve for each year between 2011 and 2023.

in the amplitude of the seasonal cycle of C_3H_8 explained by Angot et al. (2021) as a result of the increase in anthropogenic ON&G activities rather than by biomass burning (BB) emissions or OH sink, could not be a robust explanation for the main behavior recorded for the lower latitude station of Monte Cimone.

Table 1 shows Pearson's analyses of the hourly mean mixing ratios of C₃H₈, CH₄, and CO measured at Monte Cimone from 2011 to 2023. There were statistically significant positive correlations between C₃H₈ and CO, with Pearson correlation coefficients in the range of 0.44-0.61, with the highest values in spring and winter. Statistically significant positive Pearson correlation values were up to 0.38 between C₃H₈ and CH₄. Zhou et al. (2024) reported weak Pearson correlation between column mixing ratios of C₃H₈ and CH₄, resulting from CH₄ emissions related to landfills and livestock farming, whereas a strong Pearson correlation was reported related to shared emission sources such as O&NG activities and fossil fuel (FF) combustion. In summer, BB may be a common source of CO, CH₄, and C₃H₈. The relatively low O&NG extraction activity in the EU compared with the USA suggests that C₃H₈ emissions could be linked to BB and other anthropogenic emission activities such as FF combustion. However, it is important to point out that in summer, CMN can be more exposed to air



205

220



Table 1. The seasonal Pearson correlation coefficient for the hourly measurements of C_3H_8 with CH_4 and CO from 2011 to 2023. Statistically significant (p<0.05) values are highlighted in bold.

	Winter	Spring	Summer	Autumn
CH ₄	0.227	0.246	0.384	0.182
СО	0.580	0.609	0.442	0.449

masses from the regional PBL and that those air masses are probably well mixed once transported to the measurement site. Thus, atmospheric species emitted by different activities at regional scales could be characterized by high temporal correlation.

3.3 Diurnal variation in C₃H₈ mixing ratio

The hourly mean values of C_3H_8 mixing ratios were the highest between 14:00 and 16:00 UTC (Fig. 5). Similarly to the annual diurnal variation, the seasonal diurnal variations showed the highest hourly mean values between 14:00 and 16:00 UTC in winter and at 15:00 UTC in the other seasons (Fig. 5). The strong seasonal cycle affects the hourly means of C_3H_8 mixing ratios with the highest values in winter, ranging from 0.620 to 0.651 ppb, and the lowest in summer (0.150 to 0.210 ppb). Furthermore, the summer season showed the highest variability in diurnal variation of C_3H_8 mixing ratios, with differences (between hourly minimum and maximum) up to 28.8%, followed by the spring and autumn seasons, with variations of 18.1% and 12.1%, respectively. Winter exhibited the lowest diurnal variation, with a maximum difference of only 4.2%. The difference between winter and summer diurnal variations of airborne pollutants measured at Monte Cimone reflects a shift between convective transport from lower altitudes in the daytime and free troposphere conditions at night (Cristofanelli et al., 2016). Moreover, the enhanced OH sink-reactivity during the hot season also contributes to variations between the two seasons (Debevec et al., 2021). During the warm season, Monte Cimone is frequently affected by upslope wind intrusions, transporting boundary-layer air from the Po Valley and surrounding regions to the summit (Fischer et al., 2003; Van Dingenen et al., 2005). These intrusions are typically driven by thermally induced mountain-valley circulation and may lead to higher propane mixing ratios during daytime. Upslope intrusions become far less frequent in winter due to reduced surface heating and much shallower boundary layers, hence the lowest diurnal amplitude.

3.4 Variations in C₃H₈ mixing ratios during the 2020 COVID pandemic

The location of the Monte Cimone measurement station also allows one to investigate anomalous variations in atmospheric composition due to unprecedented changes in anthropogenic emission sources such as the COVID pandemic (Cristofanelli et al., 2021a). To investigate potential variations in C₃H₈ mixing ratios during the COVID pandemic in 2020, the mixing ratios measured in 2020 were compared with the pre-COVID (2011–2019), rebound (2021), and post-COVID (2022–2023) periods. In 2020, the C₃H₈ yearly mean mixing ratios were lower than the mean values before COVID (2011–2019), in 2021 (rebound), and following COVID (2022–2023) (Fig. 6). Kruskal-Wallis (Kruskal and Wallis, 1952) with post-hoc (Games and Howell, 1976) test was applied for testing the null hypothesis that a significant difference exists among the population medians





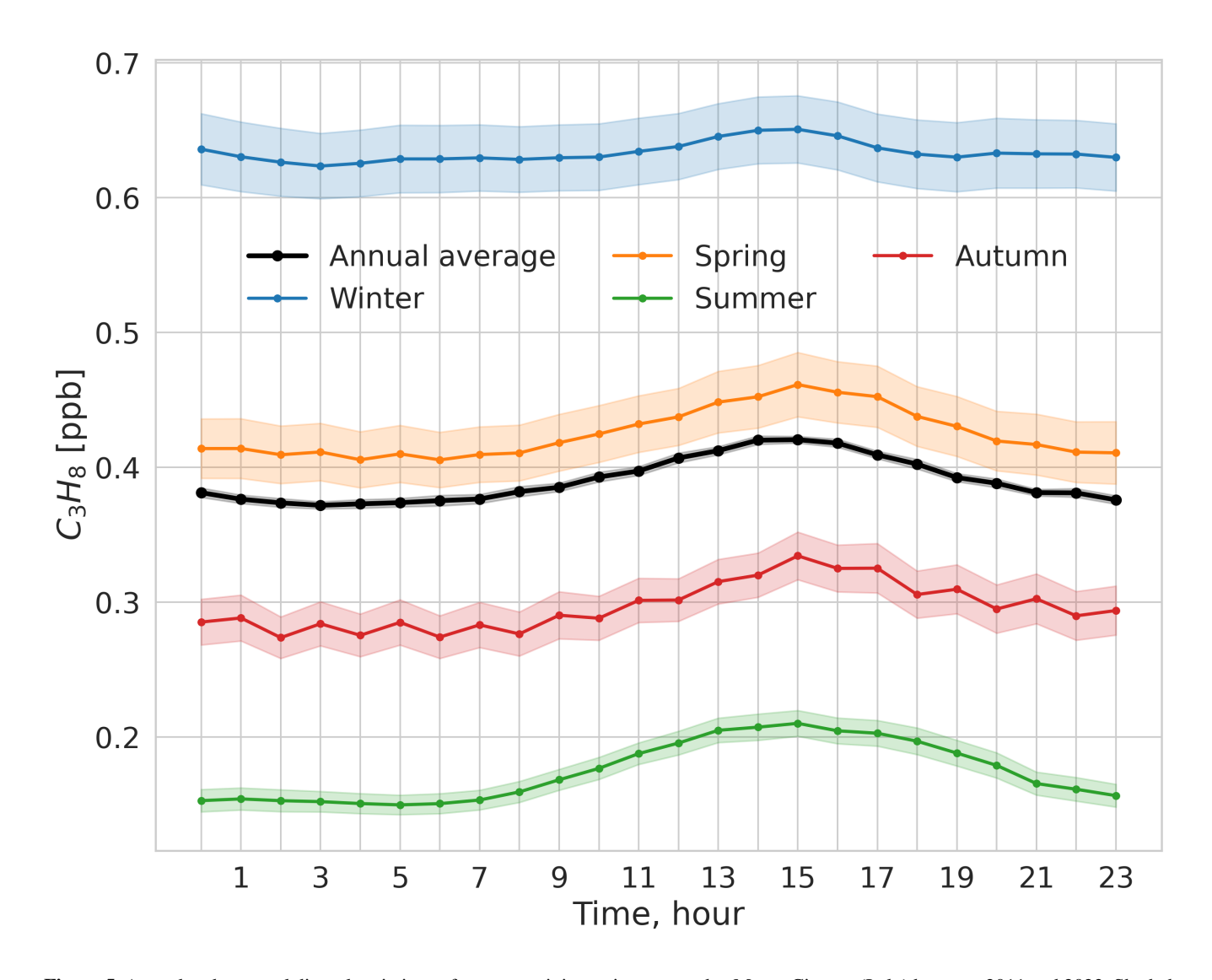


Figure 5. Annual and seasonal diurnal variations of propane mixing ratio measured at Monte Cimone (Italy) between 2011 and 2023. Shaded lines show 95% confidence interval. Smoothing consists of a 3-hour centered moving average.



225

230

235

240



of the groups. This test showed significant (p<0.05) differences between the group means (pre-COVID, COVID, rebound, and post-COVID times) apart from the pairs pre-COVID and rebound, pre-COVID and post-COVID times. Specifically, comparisons of seasonal C₃H₈ mean values showed statistical differences between pre-COVID and COVID both in summer and winter (Fig. A3). The restriction measures were generally set in late February 2020 in Italy and in the following months in the EU. Therefore, the lower mean values of C₃H₈ in winter 2020 compared to pre-COVID are not related to the COVID restrictions in the EU. For the lower values in summer 2020, our results align with the findings by Putero et al. (2023) who suggested a link between decreases in O₃ mixing ratios measured at high-elevation sites and lower emissions of O₃ precursors. The main drivers of variations in atmospheric C₃H₈ mixing ratios are changes in emission sources, atmospheric chemistry, and transport. In 2020, variations in sources of anthropogenic emissions were likely to occur due to variations in demand for O&NG products. In this context, in the European Union the final energy consumption was 2.5% and 10.4% lower for natural gas and oil and petroleum products, respectively, in 2020 compared to 2019 (https://ec.europa.eu/eurostat/statistics-explained/index.php?title= Oil_and_petroleum_products_-a_statistical_overview). Lyon et al. (2021) related the decrease in methane emissions from an oil basin in the USA to the decrease in the development activities of oil wells with the shock in the oil market during the COVID crisis. According to Cristofanelli et al. (2021a), the decreases in anthropogenic emissions of O₃ precursors, such as propane, played a role in the negative anomalies observed in monthly mean O₃ mixing ratios between spring and summer 2020 with respect to 2015-2019 at Monte Cimone. In addition, comparisons of aircraft campaign measurements across Europe showed lower OH mixing ratios in the free troposphere during the COVID-19 lockdown compared to previous campaigns performed between 2003 and 2006 (Nussbaumer et al., 2022). The expected longer residence time due to the lower reaction rate between C₃H₈ and OH is then in contrast with the lower C₃H₈ concentrations recorded at CMN in 2020, which is likely imputable to reduced emissions.

3.5 Identification of events with high C₃H₈ daily mean mixing ratios

We analysed air mass transport and associated local meteorological variables for selected high mixing ratio episodes. These events with high C₃H₈ mixing ratios were identified as days when the daily mean exceeded the 96th percentile of seasonal daily mean mixing ratios, following Cristofanelli et al. (2021b). The occurrence of events with high C₃H₈ mixing ratios was relatively evenly distributed among the years, apart from 2013, 2015, 2018, and 2023, with 11-15% of the days with high C₃H₈ mixing ratios (Tab. 2). Single-day events were from 6% (in spring) to 25% (in autumn) of the events with high C₃H₈ daily mean mixing ratios. The events lasting two or more consecutive days were between 6% (in autumn) and 11% (in spring) of the events with high C₃H₈ daily mean mixing ratios. Apart from summer, the C₃H₈ high events were characterised by lower air temperature, lower atmospheric pressure, and higher wind speed with respect to the days with ordinary daily mean C₃H₈ mixing ratios (Fig. A4). Cristofanelli et al. (2021b) observed similar atmospheric conditions for NO₂ pollution events recorded at Monte Cimone from 2015 to 2019, suggesting a role of air mass transport triggered by favorable synoptic-scale conditions.





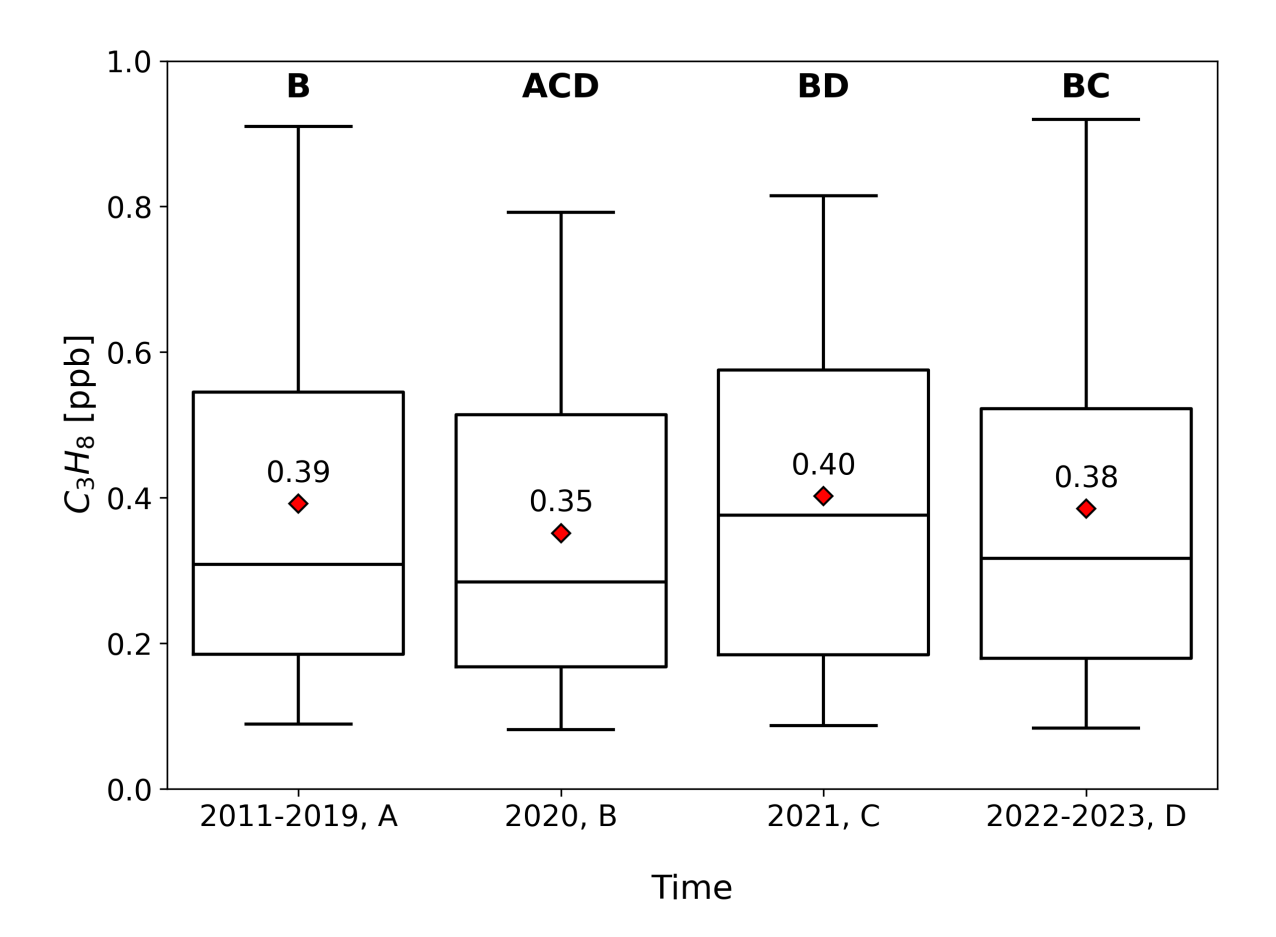


Figure 6. Boxplots of propane mixing ratios measured at Mt. Cimone before COVID (2011–2019, A), during COVID (2020, B), rebound (2021, C), and post-COVID (2022–2023, D). Boxplots show the minimum, 25%, 50%, 75% percentiles of the data, and the maximum. Red diamonds show mean values. Bold labels report the pairs that have statistically significantly different medians as a result of the pairwise post-hoc test.



265

270



Table 2. Temporal distribution of high C₃H₈ daily mean mixing ratios.

	Winter	Spring	Summer	Autumn	Whole year
2011	1	6	2	1	10
2012	7	0	0	2	9
2013	4	0	5	7	16
2014	3	3	1	2	9
2015	3	0	14	3	20
2016	0	3	2	1	6
2017	2	0	2	5	9
2018	9	7	0	7	23
2019	1	1	3	0	5
2020	0	7	0	1	8
2021	1	0	0	3	4
2022	2	6	2	4	14
2023	7	4	7	0	18
Whole period	40	37	38	36	151

55 3.5.1 Analysis of selected events with high C_3H_8 daily mean mixing ratios

Among the years with the highest number of high-mixing-ratio events, 2022 is the only one with these events in all seasons. As an example of analysis of atmospheric transport of air masses to Monte Cimone during high mixing ratio events, we performed FLEXPART simulations to compute sensitivity to the source regions for the year 2022. Figure 7 presents the mean sensitivity of Monte Cimone to source regions within the study domain for each season in 2022. The seasonal sensitivity patterns show clear differences across the year. Regardless of the season, Monte Cimone was predominantly influenced by air masses originating from the central European continent and the western Mediterranean basin. During winter, the site was affected by long-range transported air masses, with low-sensitivity values extending over a broad area, including parts of North America and Scandinavia. In contrast, summer low-sensitivity regions were more confined, primarily over the Atlantic Ocean and along the western coasts of North Africa. In spring, the station received a greater contribution from air masses originating in Eastern Europe compared to other seasons.

Figure 8 displays the emission sensitivity $(sm^{-3}kg^{-1})$ anomalies for four selected high-mixing ratio episodes, relative to the seasonal mean sensitivities (for the corresponding season in which the events occurred). Figure 8a illustrates the anomaly for a two-day event on March 11–12, 2022. The sensitivity anomaly map shows that the air masses arriving at the station during this period primarily originated from Eastern Europe, Russia, and parts of Scandinavia. Two distinct sensitivity hotspots are also visible over the North Atlantic Ocean for this episode. Figure 8b presents a similar event that occurred on March 18–21, 2022. During this episode, the air masses reaching the station were mainly from Eastern Europe and Russia. Figure 8c shows





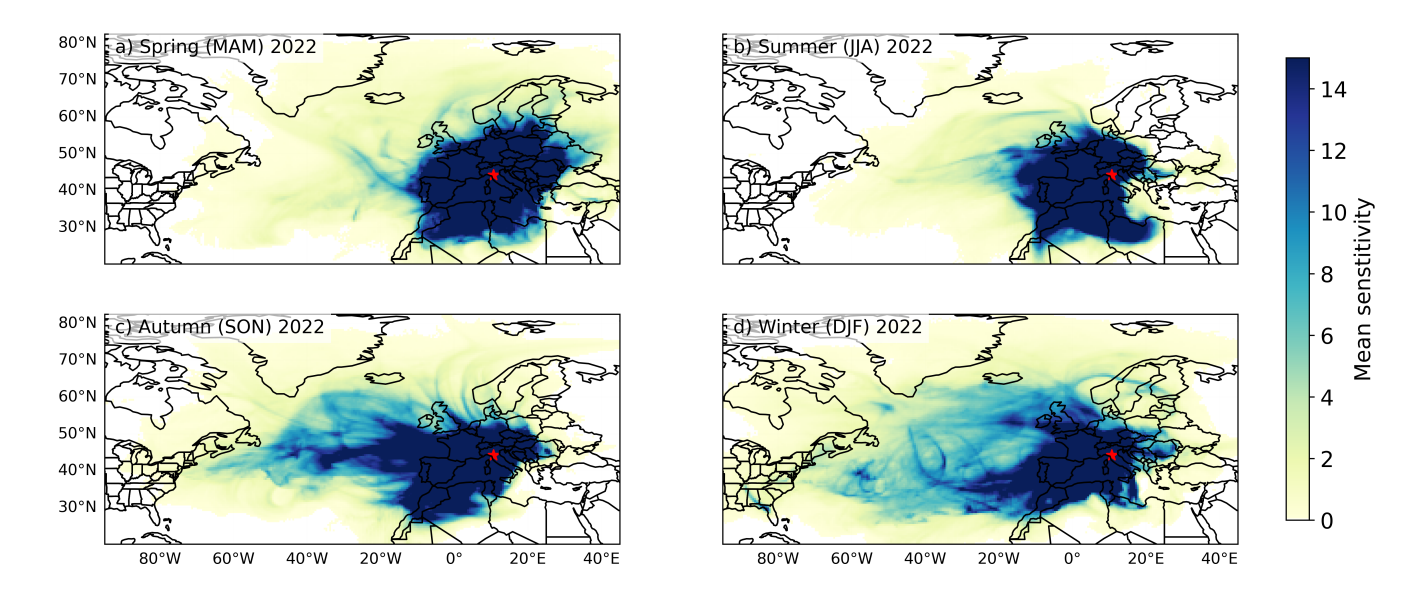


Figure 7. Seasonal mean sensitivity fields indicating the origin of air parcels reaching Monte Cimone (highlighted by a red star), derived by 5-day back-trajectory calculations performed using the FLEXPART model for the year 2022.

a three-day event in winter from November 29 to December 1, 2022. The sensitivity anomalies suggest that southeastern and parts of central Europe significantly influenced the high-mixing ratio episode during this period. Comparisons of time series of hourly means of C₃H₈, CH₄, and CO mixing ratios show a recurring pattern consisting of paired peaks and lows (Figs. A5, A6, and A7) for the events characterised by transport of air masses from Eastern Europe and Russia according to the sensitivity anomaly maps (Fig.8a, b, and c). Figure 8d depicts a four-day high-mixing ratio event that took place from February 2 to 5, 2023. For this event, the air masses arriving at the station originated from the eastern coast of the United States, the Baltic Sea, and Scandinavia, regions known for their natural gas and oil extraction activities. This event showed a C₃H₈ mixing ratio trend opposite to CH₄ and CO mixing ratios (Fig. A8).

3.6 Inversion estimates

280

285

To evaluate the consistency of the inversion system, we compared the prior and posterior mixing ratios against the observed propane mixing ratios at CMN and JFJ. Figure 9 shows that the prior mixing ratios systematically underestimate the observations, with normalised mean bias (NMB) values of –39% at CMN and –47% at JFJ. After the inversion, the agreement improves substantially, with NMB reduced to –2% at CMN and –14% at JFJ. A study by Rowlinson et al. (2024), which employed the Community Emissions Data System (CDES) inventory and the GEOS-Chem model to analyse global VOC emissions in a 2-year period (2016-2017), reported propane prior NMB values of –58% at CMN and –65% at JFJ. Their re-speciation approach based on detailed regional NMVOC estimates slightly improved the posterior NMB to -39% and -43%. In our analysis, the





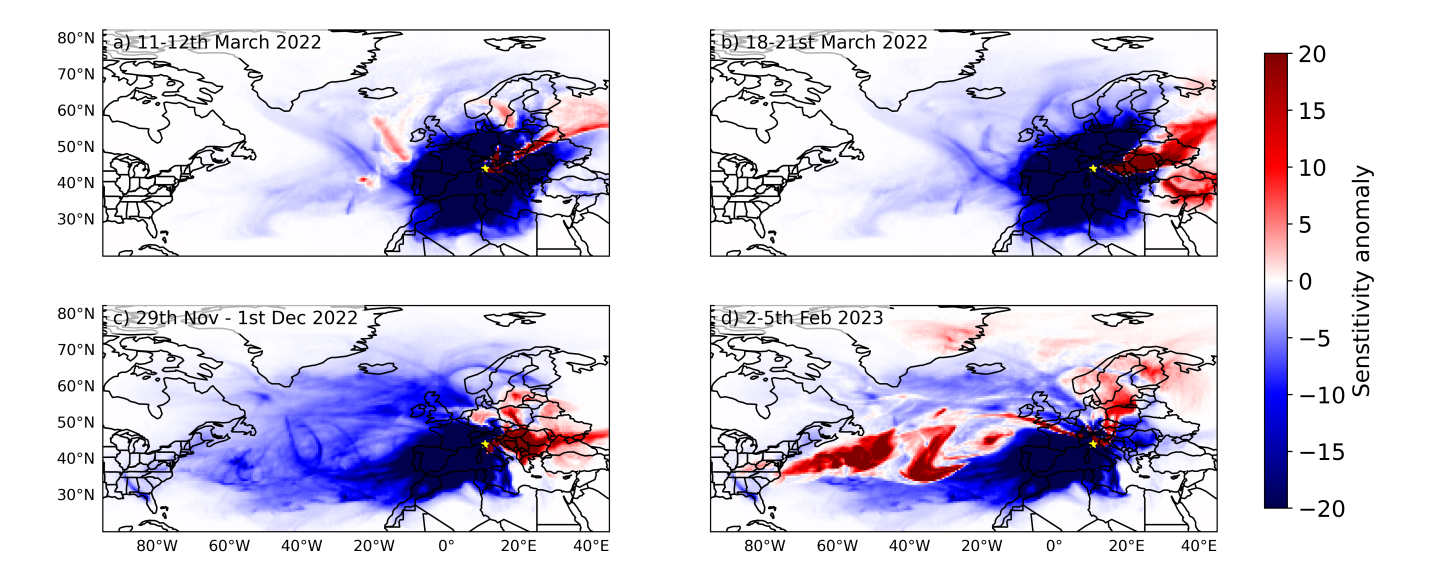


Figure 8. Sensitivity anomaly for four high-mixing ratio propane episodes. The plots show the difference between the sensitivity calculated for the pollution event and the related seasonal sensitivity (Fig. 7).

Pearson's correlation coefficients (R) between observed and prior modelled mixing ratios were 0.67 for CMN and 0.64 for JFJ, which improved to 0.80 and 0.72, respectively, after the inversion.

Figure 10 illustrates that the prior C_3H_8 emissions are substantially underestimated for Italy and France, while Swiss emissions are more accurately represented in the inventory. Our inversion yields posterior emissions for 2022 of 75.29 ± 2.00 Gg for Italy, 2.19 ± 0.41 Gg for Switzerland, and 53.06 ± 2.50 Gg for France. These correspond to increases of 224% and 137% over the EDGARv8.1 prior estimates for Italy and France, respectively, posing the question about possible relevant underestimated emissions from some sectors or the likelihood of missing sources in the EDGAR database, such as the captured sources in the south of Italy (Figure 11), where several of the main petrochemical plants are located Similar conclusions were derived by Rowlinson et al. (2024), where improvements based on re-speciation of inventories with detailed regional information were mainly for ethane, leaving some uncertainties for propane.

4 Conclusions

290

295

300

Propane (C₃H₈) is a key non-methane hydrocarbon with significant implications for tropospheric chemistry, particularly as a precursor to ozone and secondary organic aerosol formation and participating to the global atmospheric oxidative capacity by reacting with hydroxyl radicals, thereby influencing methane lifetime and background ozone levels, with implications for both climate forcing as a greenhouse gas and air quality.

This study presents the analysis of a 13-year time series of continuous measurements of C_3H_8 conducted at the WMO-GAW station of Monte Cimone. Hourly means of C_3H_8 mixing ratios followed a diurnal trend with peaks between 14:00 and 16:00





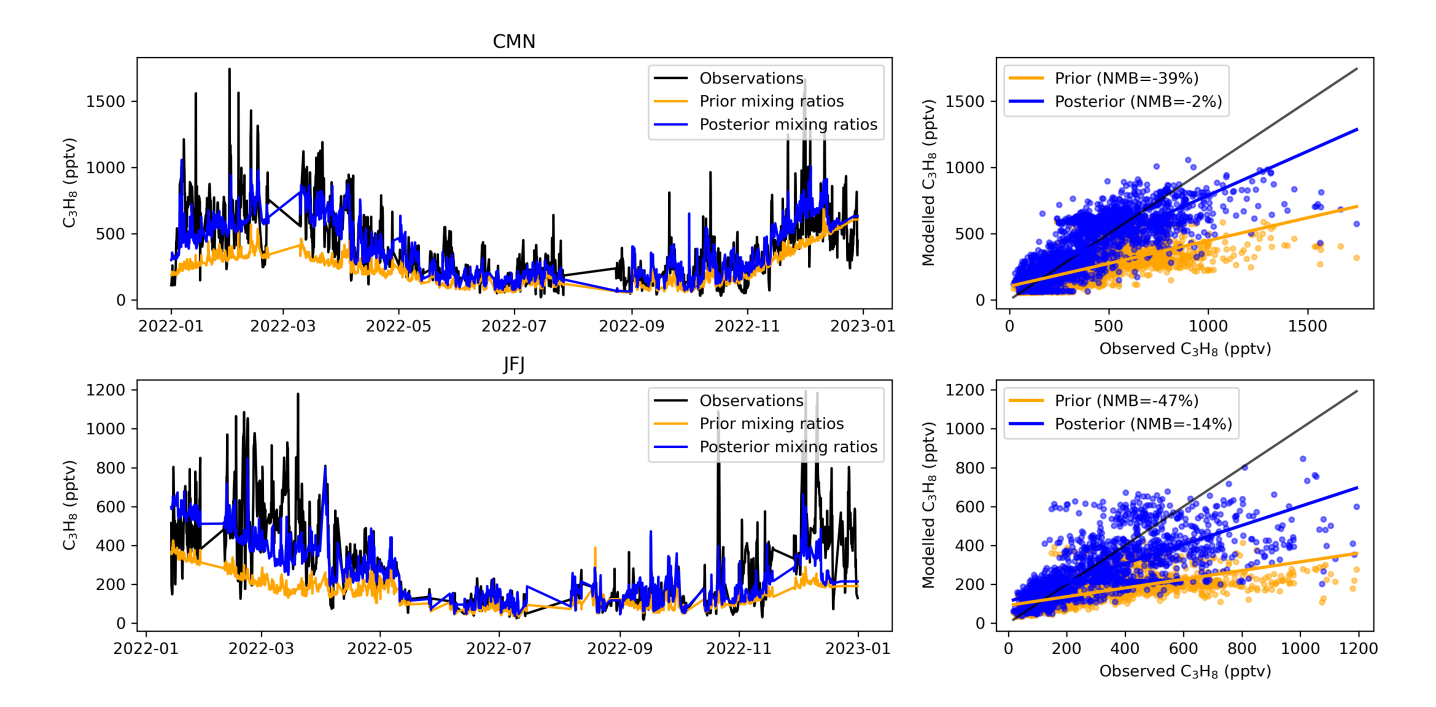


Figure 9. C₃H₈ observed (black) 3-hourly mixing ratios at CMN and JFJ sites compared with prior mixing ratios using EDGAR emissions (orange) and posterior mixing ratios (blue).

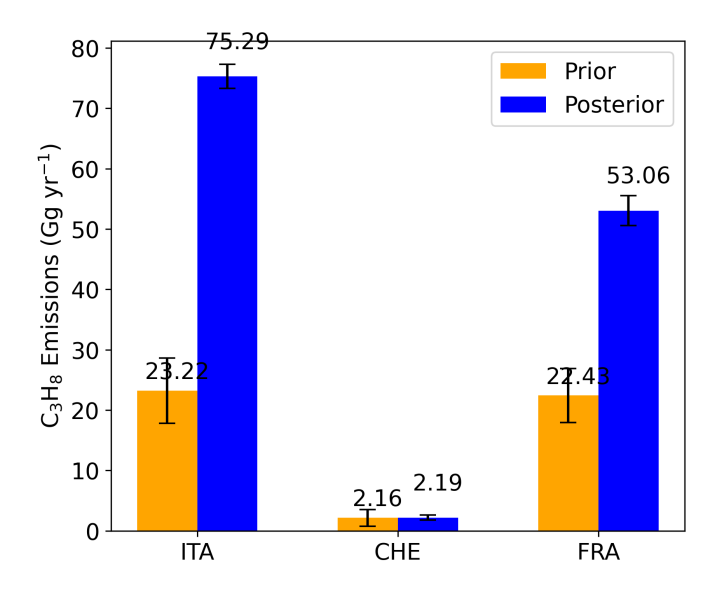


Figure 10. Prior and posterior emissions estimates of C_3H_8 for Italy (ITA), Switzerland (CHE), and France (FRA). Error bars indicate 1σ uncertainty.



320



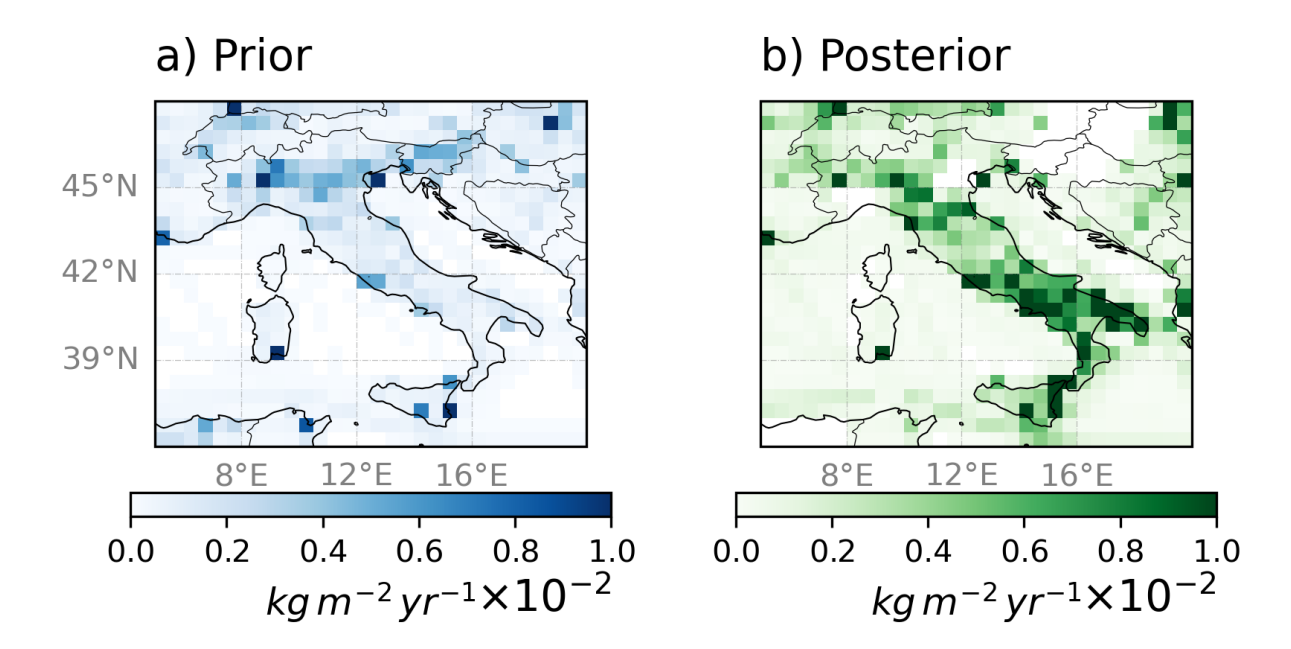


Figure 11. Spatial distribution of prior (EDGARv8.1) and posterior emissions estimates of C₃H₈ for Italy in 2022.

305 UTC and a seasonal trend, with the highest values in winter and the lowest in summer. Moreover, the variability in hourly means of C_3H_8 mixing ratios was the lowest in winter and the highest in summer.

In spring and winter, there were strong positive Pearson's correlation coefficients between C₃H₈ and CO, likely due to common anthropogenic emission sources or mixing of anthropogenic sources along the transport path.

No clear C_3H_8 long-term trend could be inferred between 2011 and 2023 with a slight decrease of -0.003 [-0.004; -0.002; 95% confidence interval] ppb per year. However, it is worth pointing out that the C_3H_8 trend exhibited a 21-month-long significant decrease and a 17-month-long significant increase up to 0.06 ppb each between July 2018 and February 2023, with the minimum centered around 2020-2021, in correspondence with the COVID period.

During the COVID pandemic, C_3H_8 yearly mean mixing ratio was lower than the mean values before COVID (2011–2019), likely due to decreases in anthropogenic emissions.

The amplitude of the C_3H_8 seasonal cycle showed an increase of about 0.16% per year from 77.5 to 79.5% in the study period, with most of the increase between 2016 and 2023, likely driven by an increase in emissions from combustion activities.

Consistent negative differences between the 2022 prior and posterior emissions of C_3H_8 for France and Italy rose from atmospheric inversion estimates performed for the countries with relatively high sensitivity to Monte Cimone and Jungfraujoch (Switzerland) stations, namely France, Italy, and Switzerland. This suggests revising the EDGAR emissions inventory for overlooked C_3H_8 emissions sources and activities. Also in view of recent disruption in the European energy mix, the estimates of C_3H_8 at the national level should adopt both bottom-up and top-down inverse modeling based on atmospheric measurements





methods to underscore the utility of C₃H₈ both as a diagnostic tracer of O&NG emissions and as an indicator of the broader impacts of energy sector practices on atmospheric composition. The results achieved by this work are mainly constrained by the limited availability of the measurements dataset for the European domain. Therefore, it is crucial to put additional effort into the monitoring activities at different scales to further our understanding of the atmospheric abundances and emissions of C₃H₈, its role in the atmospheric chemistry, and its environmental effects.



330



Code and data availability. The propane data used in this study are accessible through EBAS-ACTRIS online repository https://ebas.nilu.no/ Inverse modeling code and data availability: Code availability: The code for FLEXPART is made available under the GNU General Public License v3.0 or later from https://flexpart.img.univie.ac.at. The FLEXINVERT source code (including the preprocessors) is available from the NILU GitLab repository from https://git.nilu.no/flexpart/flexinvertplus/-/releases/v1.0.0. The model parameterizations and outputs are available upon request.





Appendix A: Monthly statistics

A1





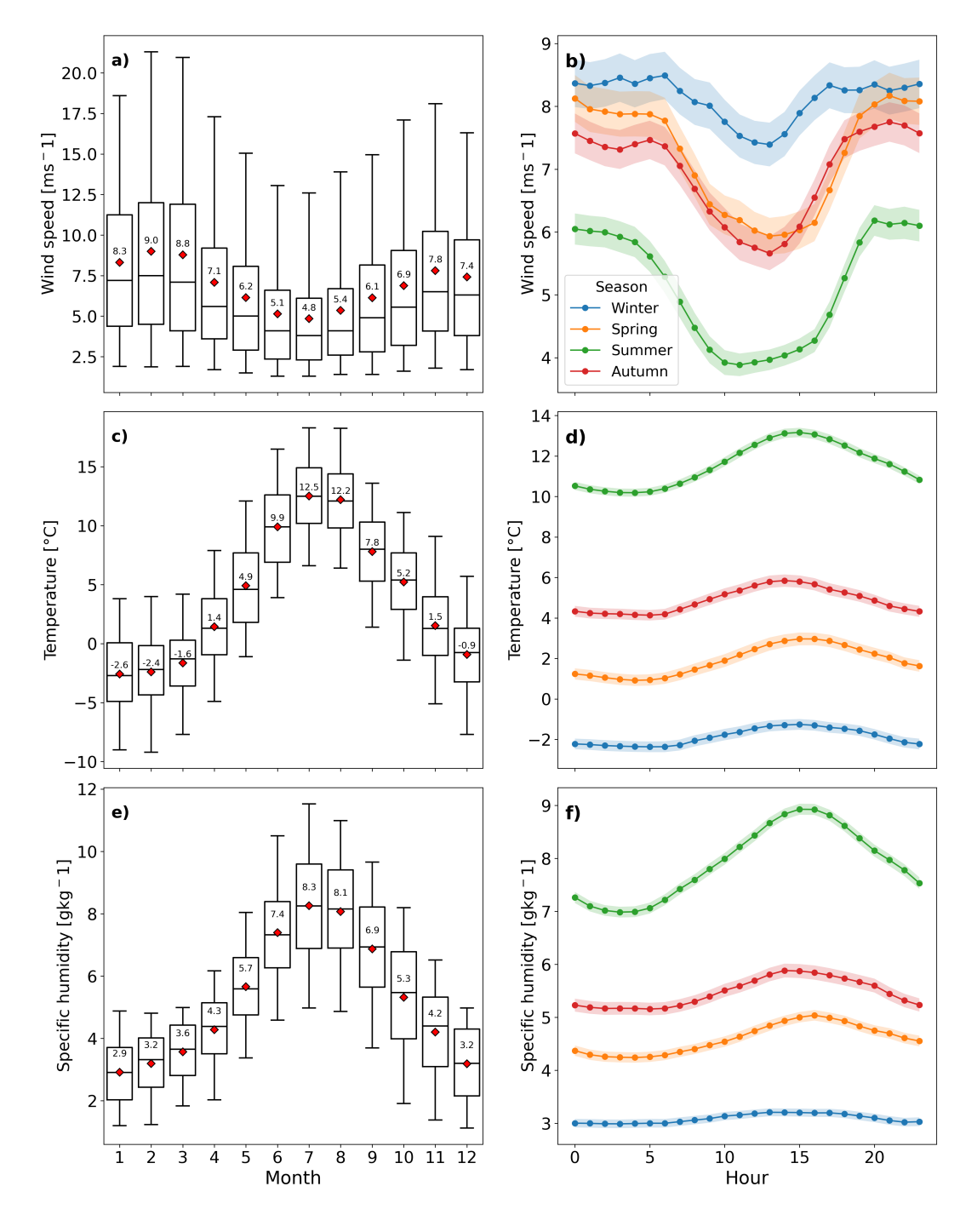


Figure A1. Monthly box plots (a, c, and e) and seasonal diel variation (b, d, and f) in wind speed (first line), temperature (central line), and specific humidity (third line) at Monte Cimone (Italy) from 2011 to 2023. From bottom to top, the horizontal lines of the box plots show the minimum, 25%, 50%, and 75% percentiles of the data, and the maximum. Red diamonds show mean values. Shaded lines show a 95% confidence interval.



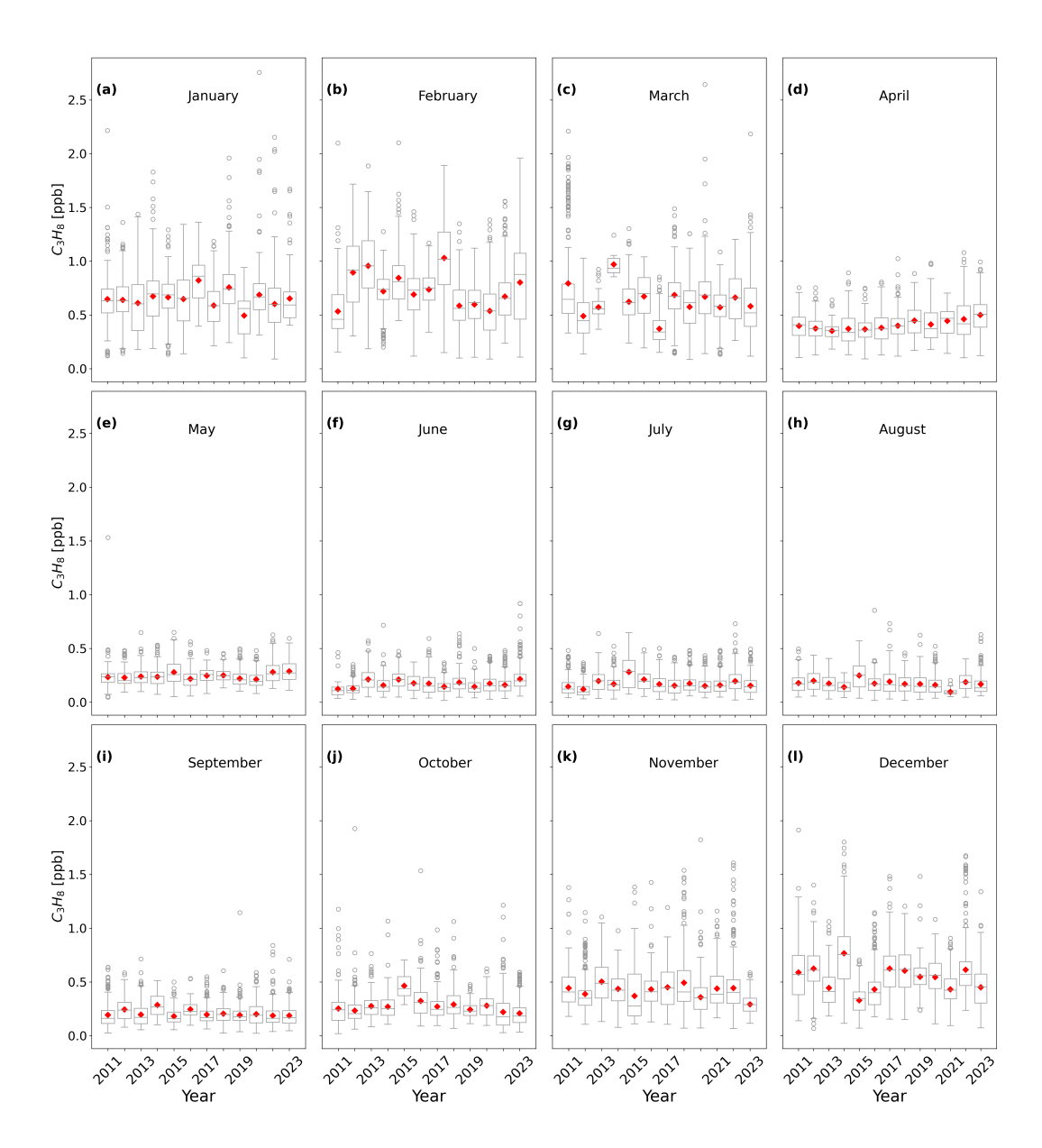


Figure A2. Boxplots of propane concentrations measured at Monte Cimone (Italy) grouped by month from 2011 to 2023. From bottom to top, the horizontal lines of the boxplots show the minimum, 25%, 50%, and 75% percentiles of the data, and the maximum. Red diamonds show mean values. Circles show outliers.





Appendix B: COVID- statistics





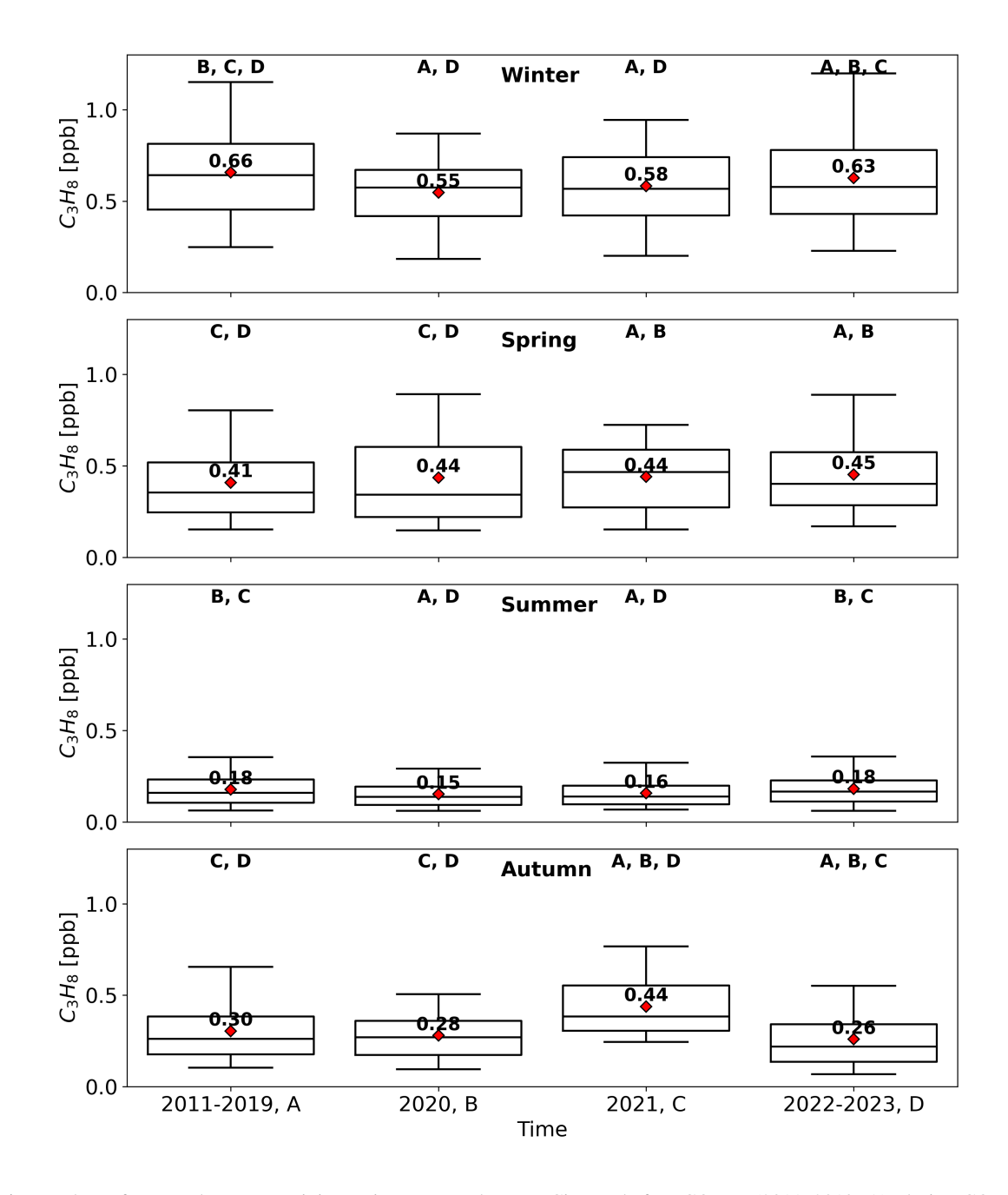


Figure B1. Boxplots of seasonal propane mixing ratios measured at Mt. Cimone before COVID (2011–2019, A), during COVID (2020, B), rebound (2021, C), and post-COVID (2022–2023, D). Boxplots show the minimum, 25%, 50%, 75% percentiles of the data, and the maximum. Red diamonds show mean values. Bold labels report the pairs that have statistically significant different medians as resulted from the pairwise post-hoc test.





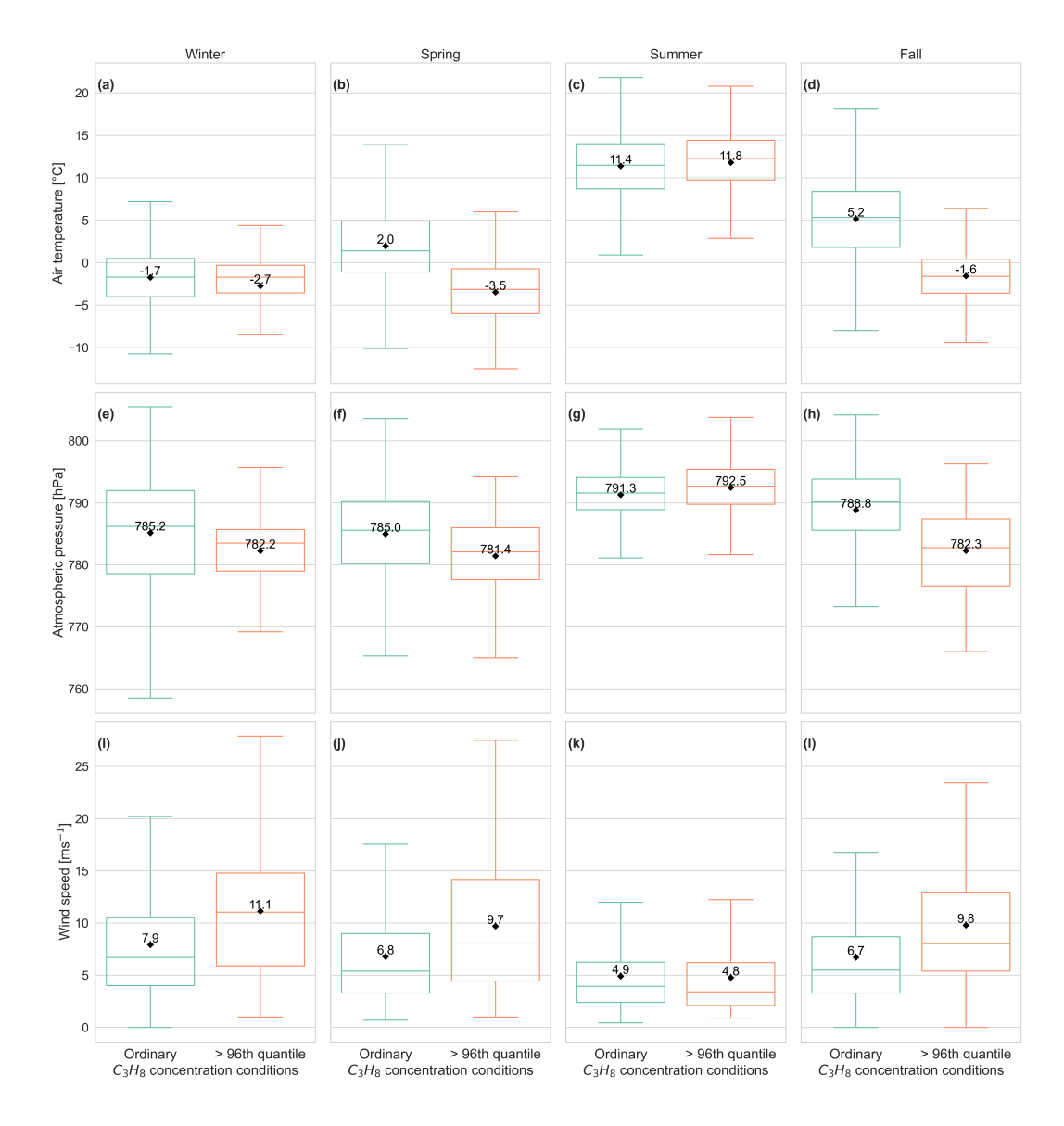


Figure C1. Comparisons between box plots of hourly measurements of air temperature (a, b, c, and d), atmospheric pressure (e, f, g, and h), and wind speed (i, j, k, and l) at Monte Cimone (Italy) grouped by seasons for the ordinary and high C_3H_8 daily mean mixing ratios from 2011 to 2023. From bottom to top, the horizontal lines of the boxplots show the minimum, 25%, 50%, and 75% percentiles of the data, and the maximum. Red diamonds show mean values.

335 Appendix C: Events - statistics





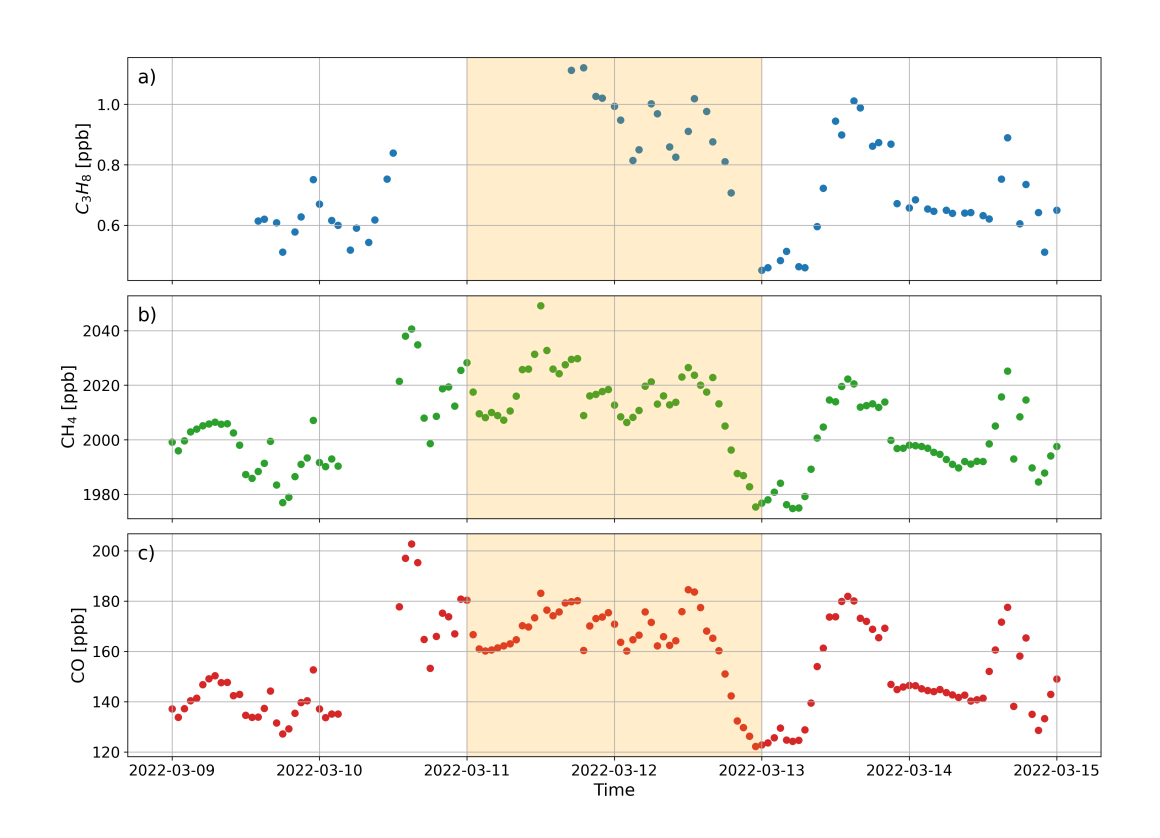


Figure C2. Time series of hourly means of a) C_3H_8 , b) CH_4 , and c) CO mixing ratios for the event occurring between March 11 and 12, 2022 (orange band) with daily mean C_3H_8 mixing ratios above the 96th percentile of the respective seasonal daily mean percentile.





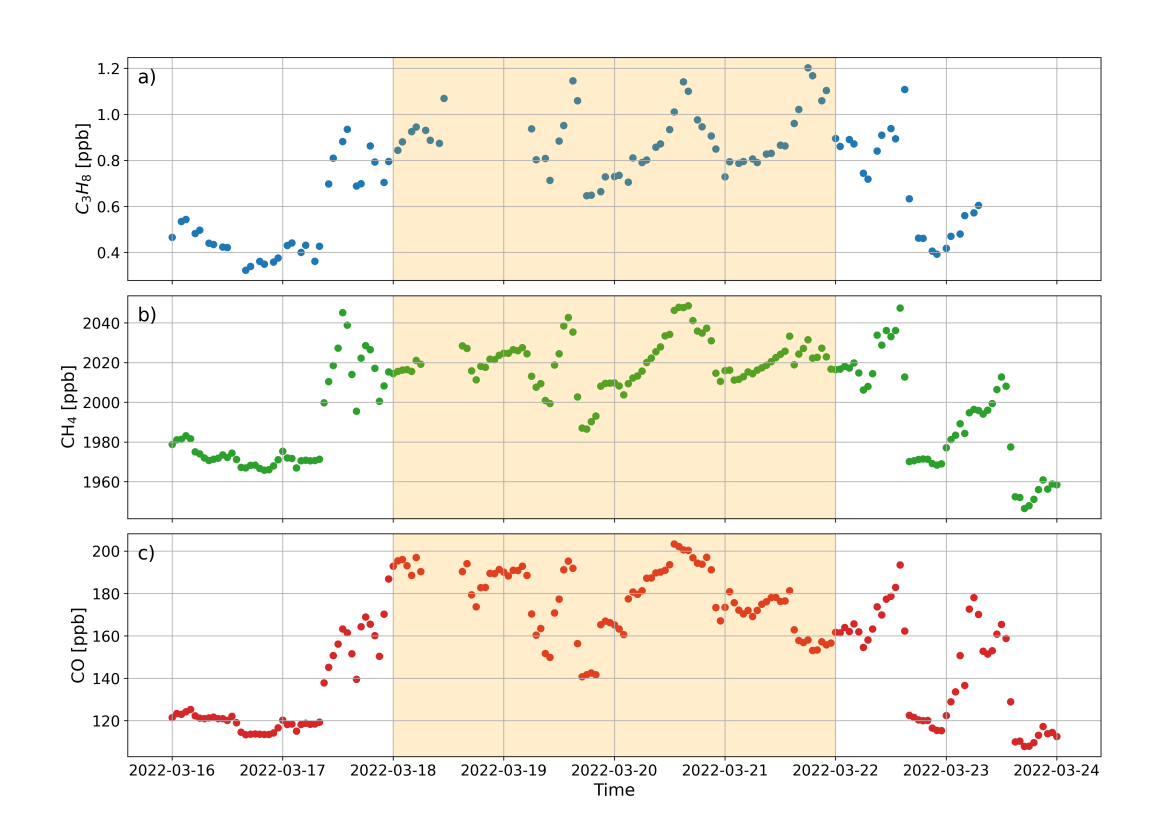


Figure C3. Time series of hourly means of a) C_3H_8 , b) CH_4 , and c) CO mixing ratios for the event occurring between March 18 and 21, 2022 (orange band) with daily mean C_3H_8 mixing ratios above the 96th percentile of the respective seasonal daily mean percentile.





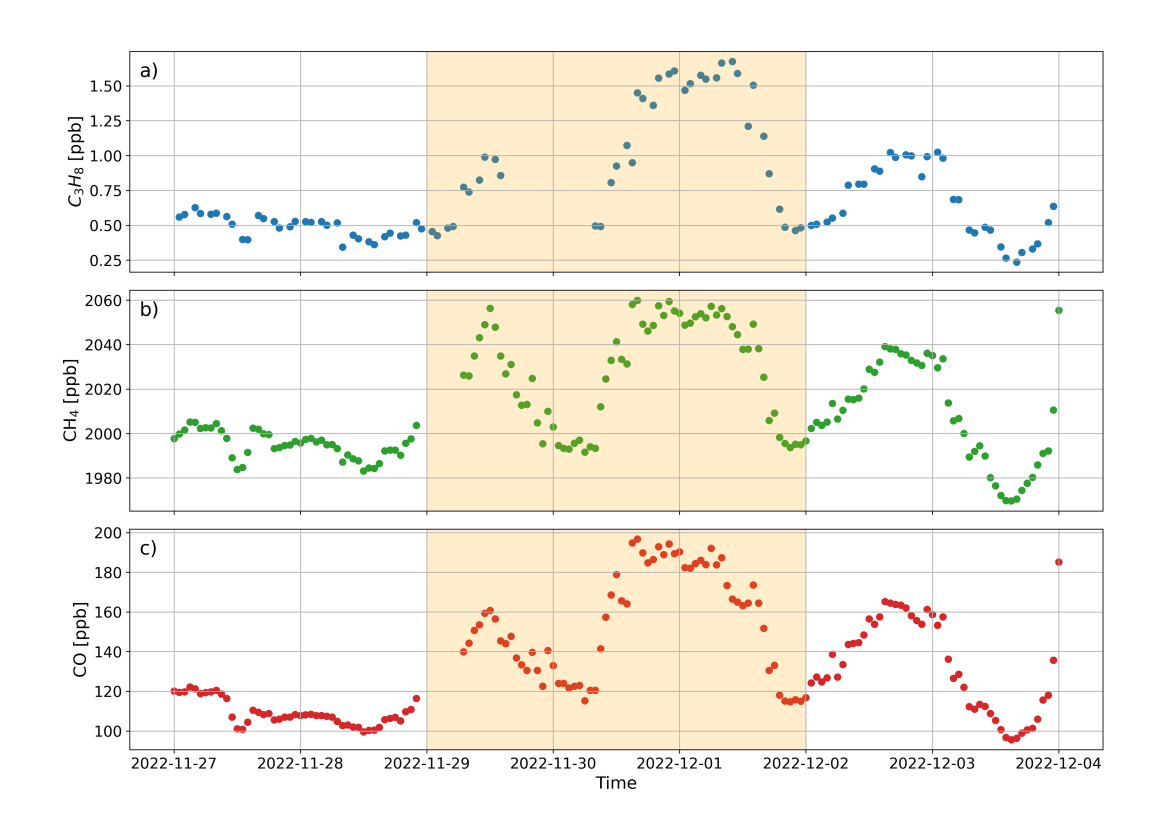


Figure C4. Time series of hourly means of a) C_3H_8 , b) CH_4 , and c) CO mixing ratios for the event occurring between November 29 and December 1, 2022 (orange band) with daily mean C_3H_8 mixing ratios above the 96th percentile of the respective seasonal daily mean percentile.





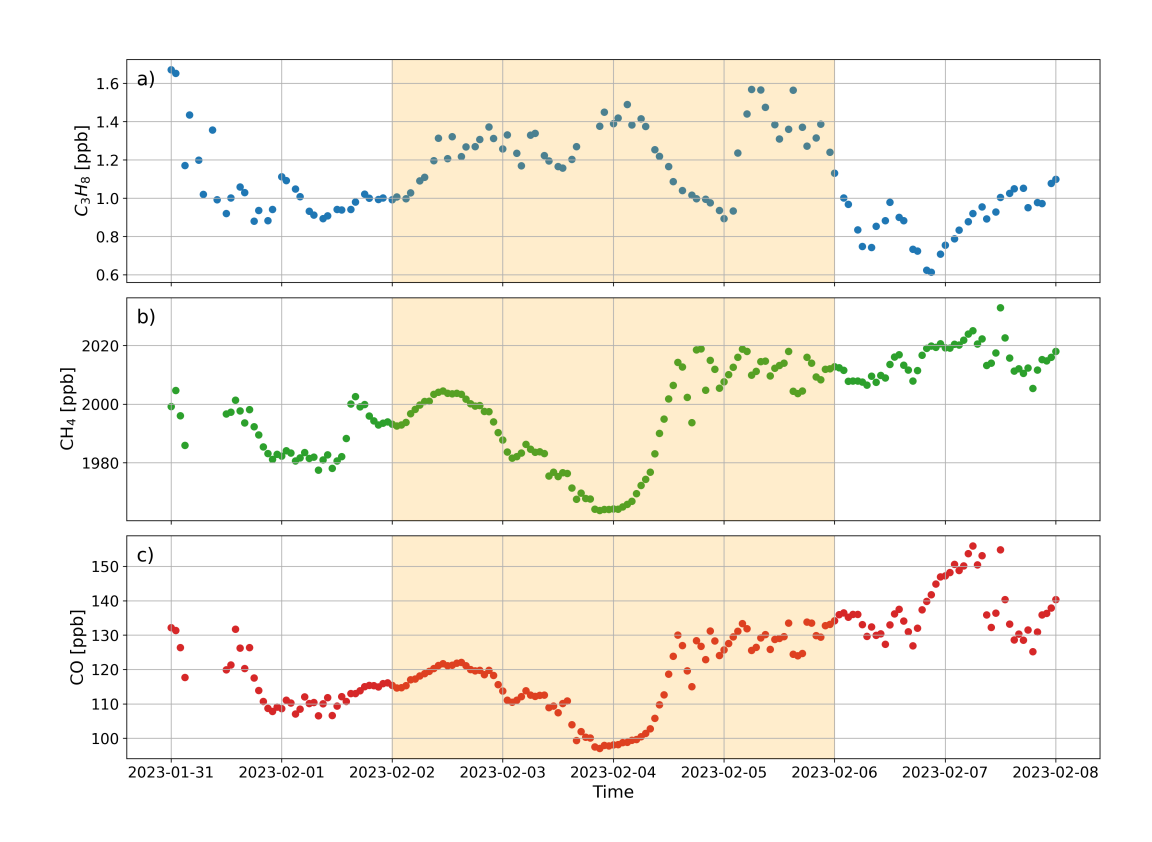


Figure C5. Time series of hourly means of a) C_3H_8 , b) CH_4 , and c) CO mixing ratios for the event occurring between February 2 and 5, 2023 (orange band) with daily mean C_3H_8 mixing ratios above the 96th percentile of the respective seasonal daily mean percentile.





Author contributions. conceptualization EM, JA, SA; Sampling, Measurements and/or analytical work are performed by JA, PC, SR; measurements data processing and quality control by JA, PC, SR; statistical data processing by EM, SA, JA; modeling work by SA; article written by EM, SA, JA with contributions from co-authors; supervision by JA, MM, UG; all authors contributed to the discussions of the results and refinement of the manuscript.

340 Competing interests. The authors declare that they have no conflict of interest.

Acknowledgements. The propane measurements at Monte Cimone was supported by FP7-Infrastructures-2010-1 grant n°262254 "ACTRIS (Aerosol, Clouds and Trace Gases Research Infrastructure)" project; the trace gas observations at Mt. Cimone has been supported by IR0000032 – ITINERIS, Italian Integrated Environmental Research Infrastructures System (D.D. n. 130/2022 - CUP B53C22002150006)

Funded by EU - Next Generation EU PNRR- Mission 4 "Education and Research" - Component 2: "From research to business" - Investment 3.1: "Fund for the realisation of an integrated system of research and innovation infrastructures" and by the Ministry for University and Researches trough the Joint Research Unit "ICOS Italy". Enrico Mancinelli's grant is funded under the Horizon Europe Project PARIS (Process Attribution of Regional Emissions, Project number 101081430). Measurements at Jungfraujoch are supported by the Swiss National Programs HALCLIM and CLIMGAS-CH (Swiss Federal Office for the Environment, FOEN), by the International Foundation High Altitude Research Stations Jungfraujoch and Gornergrat (HFSJG), and by the European infrastructure project ACTRIS and its national project ACTRIS-CH.





References

355

375

- Ali, E., Cramer, W., Carnicer, J., Georgopoulou, E., Hilmi, N., Cozannet, G. L., and Lionello, P.: Cross-Chapter Paper 4: Mediterranean Region, Climate Change 2022: Impacts, Adaptation and Vulnerability. Contribution of Working Group II to the Sixth Assessment Report of the Intergovernmental Panel on Climate Change, p. 2233–2272, 2022.
- Angot, H., Davel, C., Wiedinmyer, C., Pétron, G., Chopra, J., Hueber, J., Blanchard, B., Bourgeois, I., Vimont, I., Montzka, S. A., et al.: Temporary pause in the growth of atmospheric ethane and propane in 2015-2018, Atmospheric Chemistry and Physics, 21, 15153–15170, 2021.
- Annadate, S., Falasca, S., Cesari, R., Giostra, U., Maione, M., and Arduini, J.: A sensitivity study of a Bayesian inversion model used to estimate emissions of synthetic greenhouse gases at the European scale, Atmosphere, 15, 51, 2023.
 - Annadate, S., Mancinelli, E., Gonella, B., Moricci, F., O'Doherty, S., Stanley, K., Young, D., Vollmer, M. K., Cesari, R., Falasca, S., et al.: Monitoring the impact of EU F-gas regulation on HFC-134a emissions through a comparison of top-down and bottom-up estimates, Environmental Sciences Europe, 37, 1–12, 2025.
- Atkinson, R., Baulch, D., Cox, R., Crowley, J., Hampson, R., Hynes, R., Jenkin, M., Rossi, M., Troe, J., and IUPAC, S.: Evaluated kinetic and photochemical data for atmospheric chemistry: Volume II–gas phase reactions of organic species, Atmospheric chemistry and physics, 6, 3625–4055, 2006.
 - Baek, S., Lee, S., Shin, M., Lee, J., and Lee, K.: Analysis of combustion and exhaust characteristics according to changes in the propane content of LPG, Energy, 239, 122 297, 2022.
- Bakels, L., Tatsii, D., Tipka, A., Thompson, R., Dütsch, M., Blaschek, M., Seibert, P., Baier, K., Bucci, S., Cassiani, M., et al.: FLEXPART version 11: Improved accuracy, efficiency, and flexibility, Geoscientific Model Development, 17, 7595–7627, 2024.
 - Bourtsoukidis, E., Pozzer, A., Sattler, T., Matthaios, V. N., Ernle, L., Edtbauer, A., Fischer, H., Könemann, T., Osipov, S., Paris, J.-D., et al.: The Red Sea Deep Water is a potent source of atmospheric ethane and propane, Nature Communications, 11, 447, 2020.
 - Cristofanelli, P., Scheel, H.-E., Steinbacher, M., Saliba, M., Azzopardi, F., Ellul, R., Fröhlich, M., Tositti, L., Brattich, E., Maione, M., et al.: Long-term surface ozone variability at Mt. Cimone WMO/GAW global station (2165 m asl, Italy), Atmospheric Environment, 101, 23–33, 2015.
 - Cristofanelli, P., Landi, T. C., Calzolari, F., Duchi, R., Marinoni, A., Rinaldi, M., and Bonasoni, P.: Summer atmospheric composition over the Mediterranean basin: Investigation on transport processes and pollutant export to the free troposphere by observations at the WMO/GAW Mt. Cimone global station (Italy, 2165 m asl), Atmospheric Environment, 141, 139–152, 2016.
- Cristofanelli, P., Arduni, J., Serva, F., Calzolari, F., Bonasoni, P., Busetto, M., Maione, M., Sprenger, M., Trisolino, P., and Putero, D.:

 Negative ozone anomalies at a high mountain site in northern Italy during 2020: a possible role of COVID-19 lockdowns?, Environmental Research Letters, 16, 074 029, 2021a.
 - Cristofanelli, P., Gutiérrez, I., Adame, J., Bonasoni, P., Busetto, M., Calzolari, F., Putero, D., and Roccato, F.: Interannual and seasonal variability of NOx observed at the Mt. Cimone GAW/WMO global station (2165 m asl, Italy), Atmospheric Environment, 249, 118 245, 2021b.
- Cristofanelli, P., Montaguti, S., and Trisolino, P.: ICOS ATC CH4 Release from Monte Cimone (8.0 m), 2018-05-03-2025-03-31, https://hdl.handle.net/11676/DLkSJNzCDlfA0JzIAZbgqzDS, 2025a.
 - Cristofanelli, P., Montaguti, S., and Trisolino, P.: ICOS ATC CO Release from Monte Cimone (8.0 m), 2018-05-03-2025-03-31, https://hdl.handle.net/11676/slwXALlojsUtOKAcbKnr1X88, 2025b.



415



- Dalsøren, S. B., Myhre, G., Hodnebrog, Ø., Myhre, C. L., Stohl, A., Pisso, I., Schwietzke, S., Höglund-Isaksson, L., Helmig, D., Reimann, S., et al.: Discrepancy between simulated and observed ethane and propane levels explained by underestimated fossil emissions, Nature Geoscience, 11, 178–184, 2018.
 - Debevec, C., Sauvage, S., Gros, V., Salameh, T., Sciare, J., Dulac, F., and Locoge, N.: Seasonal variation and origins of volatile organic compounds observed during 2 years at a western Mediterranean remote background site (Ersa, Cape Corsica), Atmospheric Chemistry and Physics, 21, 1449–1484, 2021.
- Derwent, R., Field, R., Dumitrean, P., Murrells, T., and Telling, S.: Origins and trends in ethane and propane in the United Kingdom from 1993 to 2012, Atmospheric Environment, 156, 15–23, 2017.
 - Dlugokencky, E., Masarie, K., Tans, P., Conway, T., and Xiong, X.: Is the amplitude of the methane seasonal cycle changing?, Atmospheric Environment, 31, 21–26, 1997.
- Elshorbany, Y., Ziemke, J. R., Strode, S., Petetin, H., Miyazaki, K., De Smedt, I., Pickering, K., Seguel, R. J., Worden, H., Emmerichs, T., et al.: Tropospheric ozone precursors: global and regional distributions, trends, and variability, Atmospheric Chemistry and Physics, 24, 12 225–12 257, 2024.
 - Energy, D.: Quarterly report on European gas markets, Tech. rep., European Commission, https://energy.ec.europa.eu/document/download/4aebee79-01e9-4a06-927e-8dd42fc4f9a8_en?filename=New%20Quarterly%20Report%20on%20European%20gas%20markets%20Q4%202024.pdf/, 2025.
- Fischer, H., Kormann, R., Klüpfel, T., Gurk, C., Königstedt, R., Parchatka, U., Mühle, J., Rhee, T., Brenninkmeijer, C., Bonasoni, P., et al.: Ozone production and trace gas correlations during the June 2000 MINATROC intensive measurement campaign at Mt. Cimone, Atmospheric Chemistry and Physics, 3, 725–738, 2003.
 - Games, P. A. and Howell, J. F.: Pairwise multiple comparison procedures with unequal n's and/or variances: a Monte Carlo study, Journal of Educational Statistics, 1, 113–125, 1976.
- 410 Ge, Y., Solberg, S., Heal, M. R., Reimann, S., van Caspel, W., Hellack, B., Salameh, T., and Simpson, D.: Evaluation of modelled versus observed non-methane volatile organic compounds at European Monitoring and Evaluation Programme sites in Europe, Atmospheric Chemistry and Physics, 24, 7699–7729, 2024.
 - Gialesakis, N., Kalivitis, N., Kouvarakis, G., Ramonet, M., Lopez, M., Kwok, C. Y., Narbaud, C., Daskalakis, N., Mermigkas, M., Mihalopoulos, N., et al.: A twenty year record of greenhouse gases in the Eastern Mediterranean atmosphere, Science of the Total Environment, 864, 161 003, 2023.
 - Helmig, D., Petrenko, V., Martinerie, P., Witrant, E., Röckmann, T., Zuiderweg, A., Holzinger, R., Hueber, J., Thompson, C., White, J., et al.: Reconstruction of Northern Hemisphere 1950–2010 atmospheric non-methane hydrocarbons, Atmospheric Chemistry and Physics, 14, 1463–1483, 2014.
- Helmig, D., Muñoz, M., Hueber, J., Mazzoleni, C., Mazzoleni, L., Owen, R. C., Val-Martin, M., Fialho, P., Plass-Duelmer, C., Palmer, P. I., et al.: Climatology and atmospheric chemistry of the non-methane hydrocarbons ethane and propane over the North Atlantic, Elementa, 3, 000 054, 2015.
 - Helmig, D., Rossabi, S., Hueber, J., Tans, P., Montzka, S. A., Masarie, K., Thoning, K., Plass-Duelmer, C., Claude, A., Carpenter, L. J., et al.: Reversal of global atmospheric ethane and propane trends largely due to US oil and natural gas production, Nature Geoscience, 9, 490–495, 2016.
- Hersbach, H., Bell, B., Berrisford, P., Biavati, G., Horányi, A., Muñoz Sabater, J., Nicolas, J., Peubey, C., Radu, R., Rozum, I., et al.: ERA5 hourly data on pressure levels from 1940 to present, Copernicus climate change service (c3s) climate data store (cds), 10, 24381, 2023.



435

440

455

460



- Hodnebrog, Ø., Dalsøren, S. B., and Myhre, G.: Lifetimes, direct and indirect radiative forcing, and global warming potentials of ethane (C2H6), propane (C3H8), and butane (C4H10), Atmospheric Science Letters, 19, e804, 2018.
- Hu, L., Andrews, A. E., Montzka, S. A., Miller, S. M., Bruhwiler, L., Oh, Y., Sweeney, C., Miller, J. B., McKain, K., Ibarra Espinosa, S., et al.: An Unexpected Seasonal Cycle in US Oil and Gas Methane Emissions, Environmental Science & Technology, 59, 9968–9979, 2025
 - Joshi, S., Rastogi, N., and Singh, A.: Insights into the formation of secondary organic aerosols from agricultural residue burning emissions: A review of chamber-based studies, Science of The Total Environment, p. 175932, 2024.
 - Kim, K. H., Chun, H.-H., and Jo, W. K.: Multi-year evaluation of ambient volatile organic compounds: temporal variation, ozone formation, meteorological parameters, and sources, Environmental monitoring and assessment, 187, 1–12, 2015.
 - Kruskal, W. H. and Wallis, W. A.: Use of ranks in one-criterion variance analysis, Journal of the American statistical Association, 47, 583–621, 1952.
 - Lan, X., Tans, P., Sweeney, C., Andrews, A., Dlugokencky, E., Schwietzke, S., Kofler, J., McKain, K., Thoning, K., Crotwell, M., et al.: Long-term measurements show little evidence for large increases in total US methane emissions over the past decade, Geophysical Research Letters, 46, 4991–4999, 2019.
 - Lelieveld, J., Gromov, S., Pozzer, A., and Taraborrelli, D.: Global tropospheric hydroxyl distribution, budget and reactivity, Atmospheric Chemistry and Physics, 16, 12 477–12 493, 2016.
 - Li, M., Pozzer, A., Lelieveld, J., and Williams, J.: Northern hemispheric atmospheric ethane trends in the upper troposphere and lower stratosphere (2006–2016) with reference to methane and propane, Earth System Science Data, 14, 4351–4364, 2022.
- Liu, G., Shen, L., Ciais, P., Lin, X., Hauglustaine, D., Lan, X., Turner, A. J., Xi, Y., Zhu, Y., and Peng, S.: Trends in the Seasonal Amplitude of Atmospheric Methane, Nature, 641, 660–665, https://doi.org/10.1038/s41586-025-08900-8, 2025.
 - Lo Vullo, E., Furlani, F., Arduini, J., Giostra, U., Graziosi, F., Cristofanelli, P., Williams, M. L., and Maione, M.: Anthropogenic non-methane volatile hydrocarbons at Mt. Cimone (2165 m asl, Italy): Impact of sources and transport on atmospheric composition, Atmospheric Environment, 140, 395–403, 2016.
- 450 Lyon, D. R., Hmiel, B., Gautam, R., Omara, M., Roberts, K. A., Barkley, Z. R., Davis, K. J., Miles, N. L., Monteiro, V. C., Richardson, S. J., et al.: Concurrent variation in oil and gas methane emissions and oil price during the COVID-19 pandemic, Atmospheric Chemistry and Physics, 21, 6605–6626, 2021.
 - Maione, M., Giostra, U., Arduini, J., Furlani, F., Graziosi, F., Lo Vullo, E., and Bonasoni, P.: Ten years of continuous observations of stratospheric ozone depleting gases at Monte Cimone (Italy) Comments on the effectiveness of the Montreal Protocol from a regional perspective, Science of The Total Environment, 445-446, 155–164, https://doi.org/https://doi.org/10.1016/j.scitotenv.2012.12.056, 2013.
 - Nussbaumer, C. M., Pozzer, A., Tadic, I., Röder, L., Obersteiner, F., Harder, H., Lelieveld, J., and Fischer, H.: Tropospheric ozone production and chemical regime analysis during the COVID-19 lockdown over Europe, Atmospheric Chemistry and Physics, 22, 6151–6165, 2022.
 - Putero, D., Cristofanelli, P., Chang, K.-L., Dufour, G., Beachley, G., Couret, C., Effertz, P., Jaffe, D. A., Kubistin, D., Lynch, J., et al.: Fingerprints of the COVID-19 economic downturn and recovery on ozone anomalies at high-elevation sites in North America and western Europe, Atmospheric chemistry and physics, 23, 15 693–15 709, 2023.
 - Riddick, S. N., Mauzerall, D. L., Celia, M., Harris, N. R., Allen, G., Pitt, J., Staunton-Sykes, J., Forster, G. L., Kang, M., Lowry, D., et al.: Methane emissions from oil and gas platforms in the North Sea, Atmospheric Chemistry and Physics, 19, 9787–9796, 2019.
 - Rosado-Reyes, C. M. and Francisco, J. S.: Atmospheric oxidation pathways of propane and its by-products: acetone, acetaldehyde, and propionaldehyde, Journal of Geophysical Research: Atmospheres, 112, 2007.





- Rowlinson, M. J., Evans, M. J., Carpenter, L. J., Read, K. A., Punjabi, S., Adedeji, A., Fakes, L., Lewis, A., Richmond, B., Passant, N., Murrells, T., Henderson, B., Bates, K. H., and Helmig, D.: Revising VOC emissions speciation improves the simulation of global background ethane and propane, Atmospheric Chemistry and Physics, 24, 8317–8342, https://doi.org/10.5194/acp-24-8317-2024, 2024.
 - Serrano-Calvo, R., Veefkind, J. P., Dix, B., de Gouw, J., and Levelt, P. F.: COVID-19 impact on the oil and gas industry NO2 emissions: A case study of the Permian Basin, Journal of Geophysical Research: Atmospheres, 128, e2023JD038 566, 2023.
- 470 Stohl, A., Seibert, P., Arduini, J., Eckhardt, S., Fraser, P., Greally, B., Lunder, C., Maione, M., Mühle, J., O'doherty, S., et al.: An analytical inversion method for determining regional and global emissions of greenhouse gases: Sensitivity studies and application to halocarbons, Atmospheric Chemistry and Physics, 9, 1597–1620, 2009.
 - Thompson, R. L. and Stohl, A.: FLEXINVERT: an atmospheric Bayesian inversion framework for determining surface fluxes of trace species using an optimized grid, Geoscientific Model Development, https://doi.org/10.5194/gmd-7-2223-2014, 10.5194/gmd-7-2223-2014, 2014.
- Thoning, K. W., Tans, P. P., and Komhyr, W. D.: Atmospheric carbon dioxide at Mauna Loa Observatory: 2. Analysis of the NOAA GMCC data, 1974–1985, Journal of Geophysical Research: Atmospheres, 94, 8549–8565, 1989.
 - Thorpe, A. K., Kort, E. A., Cusworth, D., Ayasse, A., Bue, B. D., Yadav, V., Thompson, D. R., Frankenberg, C., Herner, J., Falk, M., et al.: Methane emissions decline from reduced oil, natural gas, and refinery production during COVID-19, Environmental Research Communications, 5, 021 006, 2023.
- 480 Toon, G. C., Blavier, J.-F. L., Sung, K., and Yu, K.: Spectrometric measurements of atmospheric propane (C 3 H 8), Atmospheric Chemistry and Physics, 21, 10727–10743, 2021.
 - Tzompa-Sosa, Z. A., Henderson, B., Keller, C. A., Travis, K., Mahieu, E., Franco, B., Estes, M., Helmig, D., Fried, A., Richter, D., et al.: Atmospheric implications of large C2-C5 alkane emissions from the US Oil and Gas Industry, Journal of Geophysical Research: Atmospheres, 124, 1148–1169, 2019.
- Van Dingenen, R., Putaud, J.-P., Martins-Dos Santos, S., and Raes, F.: Physical aerosol properties and their relation to air mass origin at Monte Cimone (Italy) during the first MINATROC campaign, Atmospheric Chemistry and Physics, 5, 2203–2226, 2005.
 - Vojta, M., Plach, A., Thompson, R. L., and Stohl, A.: A comprehensive evaluation of the use of Lagrangian particle dispersion models for inverse modeling of greenhouse gas emissions, Geoscientific Model Development, 15, 8295–8323, 2022.
- Zhao, Y., Saunois, M., Bousquet, P., Lin, X., Berchet, A., Hegglin, M. I., Canadell, J. G., Jackson, R. B., Deushi, M., Jöckel, P., et al.: On the role of trend and variability in the hydroxyl radical (OH) in the global methane budget, Atmospheric Chemistry and Physics, 20, 13 011–13 022, 2020.
 - Zhou, M., Wang, P., Dils, B., Langerock, B., Toon, G., Hermans, C., Nan, W., Cheng, Q., and De Mazière, M.: Atmospheric propane (C3H8) column retrievals from ground-based FTIR observations in Xianghe, China, Atmospheric Measurement Techniques, 17, 6385–6396, 2024.